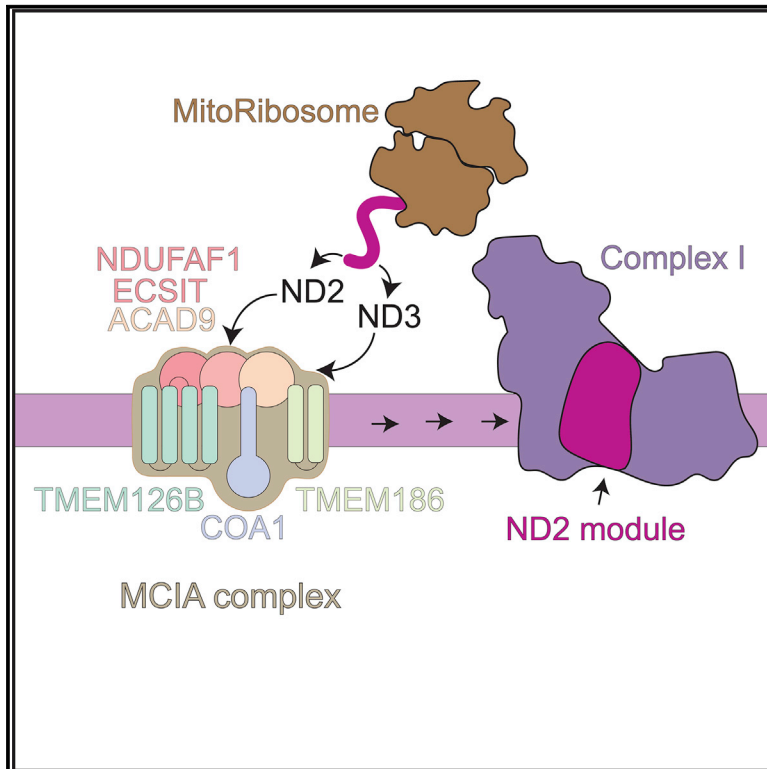


## Dissecting the Roles of Mitochondrial Complex I Intermediate Assembly Complex Factors in the Biogenesis of Complex I

### Graphical Abstract



### Authors

Luke E. Formosa, Linden Muellner-Wong, Boris Reljic, ..., Michael Lazarou, David A. Stroud, Michael T. Ryan

### Correspondence

luke.formosa@monash.edu (L.E.F.), michael.ryan@monash.edu (M.T.R.)

### In Brief

Formosa et al. investigate the function of the MCIa complex in complex I assembly. They demonstrate the requirement of individual components for the formation of complex I intermediates and assembly of the final enzyme. Finally, they characterize the involvement of TMEM186 and COA1 in this process.

### Highlights

- The MCIa complex is required for stability of mtDNA-encoded ND2
- Assembly factors show a hierarchy of stability centered on ACAD9
- TMEM186 interacts strongly with newly synthesized ND3
- COA1 interacts with newly translated ND2 and is dispensable for complex IV assembly



# Dissecting the Roles of Mitochondrial Complex I Intermediate Assembly Complex Factors in the Biogenesis of Complex I

Luke E. Formosa,<sup>1,\*</sup> Linden Muellner-Wong,<sup>1</sup> Boris Reljic,<sup>1,2</sup> Alice J. Sharpe,<sup>1</sup> Thomas D. Jackson,<sup>2</sup> Traude H. Beilharz,<sup>1</sup> Diana Stojanovski,<sup>2</sup> Michael Lazarou,<sup>1</sup> David A. Stroud,<sup>2</sup> and Michael T. Ryan<sup>1,3,\*</sup>

<sup>1</sup>Department of Biochemistry and Molecular Biology, Monash Biomedicine Discovery Institute, Monash University, Melbourne, VIC 3800, Australia

<sup>2</sup>Department of Biochemistry and Molecular Biology, The Bio21 Institute, The University of Melbourne, Melbourne, VIC 3000, Australia

<sup>3</sup>Lead Contact

\*Correspondence: [luke.formosa@monash.edu](mailto:luke.formosa@monash.edu) (L.E.F.), [michael.ryan@monash.edu](mailto:michael.ryan@monash.edu) (M.T.R.)

<https://doi.org/10.1016/j.celrep.2020.107541>

## SUMMARY

Mitochondrial complex I harbors 7 mitochondrial and 38 nuclear-encoded subunits. Its biogenesis requires the assembly and integration of distinct intermediate modules, mediated by numerous assembly factors. The mitochondrial complex I intermediate assembly (MCIA) complex, containing assembly factors NDUFAF1, ECSIT, ACAD9, and TMEM126B, is required for building the intermediate ND2-module. The role of the MCIA complex and the involvement of other proteins in the biogenesis of this module is unclear. Cell knockout studies reveal that while each MCIA component is critical for complex I assembly, a hierarchy of stability exists centered on ACAD9. We also identify TMEM186 and COA1 as bona fide components of the MCIA complex with loss of either resulting in MCIA complex defects and reduced complex I assembly. TMEM186 enriches with newly translated ND3, and COA1 enriches with ND2. Our findings provide new functional insights into the essential nature of the MCIA complex in complex I assembly.

## INTRODUCTION

Mitochondrial complex I is the first enzyme of the oxidative phosphorylation (OXPHOS) system and is required for the generation of the proton motive force driving ATP production and normal mitochondrial function (Hirst, 2013; Sazanov, 2015). In humans, complex I is composed of 45 subunits that are encoded by 44 genes, because one subunit (NDUFAF1) is located in two distinct regions of the enzyme. Complex I is encoded by both the nuclear and mitochondrial genomes and requires at least 15 assembly factors for its biogenesis (Formosa et al., 2018; Sánchez-Caballero et al., 2016a; Zhu et al., 2016). Fourteen core subunits are required for substrate oxidation, electron transport, and proton translocation. The remaining accessory/supernumerary subunits form a proteinaceous cage that surround these core subunits (Fiedorczuk et al., 2016; Zhu et al., 2016), and most are

required for assembly, stability, and hence, activity of the enzyme (Stroud et al., 2016). Complex I further assembles into higher ordered respiratory supercomplexes with complex III and complex IV (Letts et al., 2019; Schägger and Pfeiffer, 2000, 2001). The function of these supercomplexes is still under debate with proposed roles including substrate channeling, complex stability, assembly, and membrane organization (Bianchi et al., 2004; Fedor and Hirst, 2018; Guo et al., 2017; La-puente-Brun et al., 2013; Letts et al., 2016, 2019; Milenkovic et al., 2017; Protasoni et al., 2020). It has also been demonstrated that loss of complex III reduces the levels of/or impedes assembly of complex I, suggesting a dynamic interplay between the respiratory enzymes during their biogenesis (Acín-Pérez et al., 2004). Indeed, models for the assembly of the supercomplex include partially assembled complex I integrating with assembly intermediates of complexes III and IV (Moreno-Lastres et al., 2012), or assembly of complex I and IV against a complex III scaffold (Protasoni et al., 2020), while other evidence supports the formation of the supercomplex from pre-existing, fully assembled enzymes (Acín-Pérez et al., 2008; Guerrero-Castillo et al., 2017).

Complex I biogenesis requires the synthesis and inner membrane insertion of the seven core mtDNA-encoded subunits—ND1, ND2, ND3, ND4, ND4L, ND5, and ND6 (Formosa et al., 2018; Sánchez-Caballero et al., 2016a). Insertion appears to take place in a co-translational manner via the insertase OXA1L (Thompson et al., 2018). The remaining subunits are all nuclear-encoded and are imported into mitochondria. The majority are imported into the matrix where they assemble into matrix arm intermediates (Q- and N-modules), while other subunits assemble in specific modules at the membrane with mtDNA-encoded subunits (Dunning et al., 2007; Lazarou et al., 2007; Stroud et al., 2016; Ugalde et al., 2004; Vogel et al., 2007a). In cells with mutations in mtDNA-encoded subunits, a number of assembly intermediates have also been observed that accumulate with both mitochondrial and nuclear encoded subunits (Perales-Clemente et al., 2010). This includes the ND1-module (also referred to as P<sub>P</sub>-a) and ND2-module (P<sub>P</sub>-b) that are part of the proximal membrane arm and the ND4-module (P<sub>D</sub>-a) and ND5-module (P<sub>D</sub>-b) that are part of the distal membrane arm (Guerrero-Castillo et al., 2017; Sánchez-Caballero et al., 2016a). Assembly factors play a prominent role in the biogenesis of



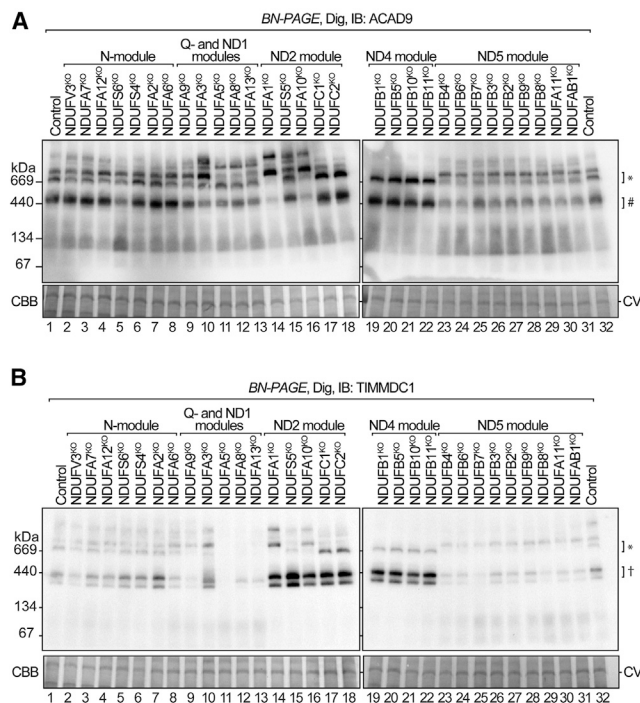


**Figure 1. Complex I Assembly Intermediates Are Disrupted in Accessory Subunit KO Mitochondria**

(A and B) Mitochondria from indicated cell lines were solubilized in digitonin and analyzed by BN-PAGE and immunoblotting (IB) for (A) ACAD9 and (B) TIMMDC1. #, ACAD9 ~450 kDa complex. †, TIMMDC1 ~400 and 440 kDa complexes. \*, ~680 and 720 kDa complexes. A portion of the Coomassie stained blot (CBB) with complex V (CV) shown serves as a loading control.

complex I and perform functions that include the post-translational modification of subunits (Rhein et al., 2013, 2016; Zurita Rendón et al., 2014), delivery of cofactors (Sheftel et al., 2009), insertion of proteins into the inner membrane, and stabilization of partially assembled, intermediate modules (Formosa et al., 2018). In cases where complex I subunits are damaged or assembly is compromised, they are degraded by mitochondrial proteases to maintain mitochondrial integrity and to prevent production of reactive oxygen species (Pryde et al., 2016; Puchades et al., 2019; Zurita Rendón and Shoubridge, 2012; Stiburek et al., 2012).

In this study, we focus on the role of the mitochondrial complex I intermediate assembly (MCIA) complex, an inner membrane machine composed of numerous assembly factors whose function is poorly understood, but converges on the biogenesis of the ND2-module. The MCIA complex is composed of core subunits NDUFAF1 (Vogel et al., 2005), ECSIT (Vogel et al., 2007b), ACAD9 (Nouws et al., 2010), and TMEM126B (Heide et al., 2012). The assembly factor TIMMDC1 has also been identified in association with the MCIA complex and stalled complex I intermediate (Andrews et al., 2013; Guarani et al., 2014). Pathogenic mutations have also been identified in NDUFAF1 (Dunning et al., 2007; Fassone et al., 2011), ACAD9 (Haack et al., 2010; Nouws et al., 2010), TMEM126B (Alston et al., 2016; Sánchez-Caballero et al., 2016b), and TIMMDC1 (Kremer et al., 2017).

In addition, complexome analysis—correlative analysis of proteins that migrate together on blue-native gels—revealed that TMEM186 and COA1 co-migrate with complex I assembly intermediates that contain known MCIA complex components (Guerrero-Castillo et al., 2017). As yet, a direct role for TMEM186 and COA1 in complex I assembly has not been experimentally validated. Here, we find the known core MCIA subunits are critical for complex I assembly with a dynamic interplay between the stability of subunits, while TMEM186 and COA1 serve important, yet more peripheral roles in assembly of the enzyme.

## RESULTS

### Loss of Complex I Accessory Subunits Perturbs Steady-State Assembly Factor Complexes

Guerrero-Castillo et al. (2017) profiled the *de novo* assembly of complex I using Blue Native (BN)-PAGE and quantitative mass spectrometry, and uncovered at least 10 distinct intermediate complexes containing various assembly factors. This included the MCIA and TIMMDC1 modules forming an intermediate containing the Q/ND1 and ND2 modules (designated Q/P<sub>P</sub>). The MCIA-ND2 module was also found in an independent ND4 assembly (P<sub>P</sub>-b/P<sub>D</sub>-a). However, under homeostatic conditions where a population of complex I and intermediates is always present, the MCIA and TIMMDC1 complexes resolve as a number of more defined complexes on BN-PAGE (Figure 1). ACAD9-containing complexes from control mitochondria consist of a major species at ~450 kDa (Figure 1A, lanes 1 and 32, marked with #) and a larger doublet of ~680 kDa and ~720 kDa (Figure 1A, lanes 1 and 32, marked with an asterisk [\*]). TIMMDC1 is found in steady-state complexes of ~400 kDa, 440 kDa (Figure 1B, lanes 1 and 32, marked with a cross [‡]), plus two larger complexes similar to that seen for ACAD9 (Figure 1B, lanes 1 and 32, \*).

We first sought to determine how these complexes were affected in mitochondria lacking individual complex I subunits belonging to defined modules that we previously characterized (Stroud et al., 2016). Loss of subunits from the NADH-dehydrogenase (N-) module did not affect the appearance of either ACAD9 or TIMMDC1 modules (lanes 2–8), supporting earlier studies that N-module assembly occurs last in assembly (Lazarou et al., 2007; Stroud et al., 2016). Although reduced in levels, the migration of these complexes was also largely unaffected in mitochondria lacking subunits belonging to the distal ND5-module (lanes 23–31). Variations were apparent in subunit knockouts (KOs) belonging to the Q, ND1, ND2, and ND4 modules. Loss of ND4-module subunits also led to loss of the higher complex for both ACAD9 and TIMMDC1 (lanes 19–22). This suggests that the higher species represents assembly factors associated in an intermediate containing the Q/ND1/ND2/ND4 module (i.e., Q/P<sub>P</sub>/P<sub>D</sub>-a). Furthermore, loss of ND4-module subunits resulted in robust accumulation of the TIMMDC1 doublet (Figure 1B, lanes 19–22, labeled with †), with similar changes observed with loss of ND2-module subunits (Figure 1B, lanes 14–18). Changes to the higher complexes containing TIMMDC1 in mitochondria lacking ND2-module subunits mirrored those observed for ACAD9, suggesting that most of these complexes represent associations between assembly factors, the ND1-module, and crippled ND2-modules. Finally, in mitochondria lacking some

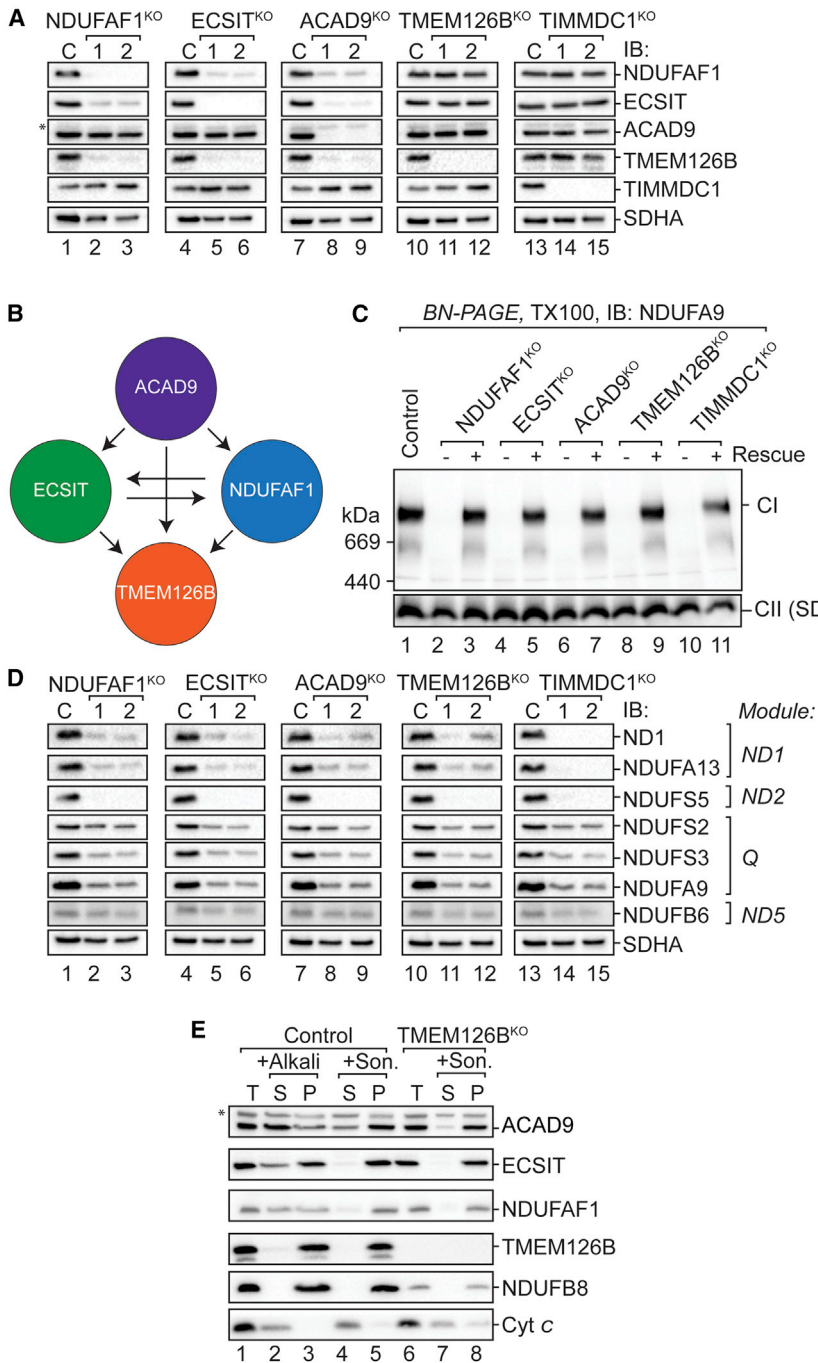


**Figure 2. MCIA Complex Subunit Hierarchy**

(A) Mitochondrial proteins from control (C) and KO cell lines were subjected to SDS-PAGE and immunoblot analysis using antibodies as indicated. SDHA served as a loading control.

(B) Schematic representation depicting the hierarchy of stability between MCIA complex components.

(C) BN-PAGE and immunoblot analysis for complex I (NDUFA9).

(D) SDS-PAGE and immunoblot analysis of complex I subunit levels in mitochondria from KO cells. (E) Mitochondria from control and TMEM126B<sup>KO</sup> cells were subjected to alkali extraction or sonication with supernatant (S) and pellet (P) fractions analyzed by SDS-PAGE and immunoblotting. See also Figure S1 and Table S1.

also absent in NDUFA8 and NDUFA13 KO mitochondria, except for a low abundant species migrating between the 400 and 440 kDa complexes. In summary, we conclude that ACAD9 and TIMMDC1 exist in independent, lower molecular weight steady-state complexes as well as together in higher molecular weight species. Our results also suggest that disruption of any single complex I assembly module can have a large effect on the behavior of other modules of the assembly pathway and may not be restricted to the modules directly affected.

### The MCIA Complex Is Crucial for Complex I Assembly

To investigate the interplay of the assembly factors, we generated KO cell lines for MCIA genes *ACAD9*, *ECSIT*, and *TMEM126B* and used these together with previously validated *NDUFAF1*<sup>KO</sup> and *TIMMDC1*<sup>KO</sup> cells (Table S1) (Stroud et al., 2016). Immunoblot analysis of two independent KO cell lines confirmed loss of the targeted gene product (Figure 2A). A dynamic interplay between the stability of other MCIA assembly factors was also observed. For example, in the absence of *NDUFAF1*, the levels of *ECSIT* and *TMEM126B* were strongly reduced relative to the control, while *ACAD9* was unchanged (Figure 2A, lanes 1–3). The *ECSIT*<sup>KO</sup> cell lines mirrored this effect pointing to the close interaction between *NDUFAF1* and *ECSIT* (Figure 2A, lanes 4–6). In the *ACAD9*<sup>KO</sup> cells, the levels of *NDUFAF1*, *ECSIT*, and *TMEM126B* were all reduced relative to the control cells (Figure 2A, lanes 7–9). However, mitochondria lacking the membrane-integrated *TMEM126B* retained normal levels of other matrix facing MCIA complex proteins (Figure 2A, lanes 10–15). Thus, the stability of *ACAD9* is independent of other known

of the Q- and ND1-module subunits, *ACAD9*-containing complexes were perturbed with loss of the accumulation of a higher molecular weight species (Figure 1A, lanes 10–13). *TIMMDC1* complexes were also absent, with the exception of *NDUFA3*<sup>KO</sup> mitochondria (Figure 1B, lanes 9–13). *TIMMDC1* complexes were also absent from *NDUFA5*<sup>KO</sup> mitochondria. *NDUFA5* is an accessory subunit of the Q-module, suggesting proper formation of the Q-module is a requirement for *TIMMDC1* to form the 400 kDa and 440 kDa complexes. *TIMMDC1* complexes were

relative to the control, while *ACAD9* was unchanged (Figure 2A, lanes 1–3). The *ECSIT*<sup>KO</sup> cell lines mirrored this effect pointing to the close interaction between *NDUFAF1* and *ECSIT* (Figure 2A, lanes 4–6). In the *ACAD9*<sup>KO</sup> cells, the levels of *NDUFAF1*, *ECSIT*, and *TMEM126B* were all reduced relative to the control cells (Figure 2A, lanes 7–9). However, mitochondria lacking the membrane-integrated *TMEM126B* retained normal levels of other matrix facing MCIA complex proteins (Figure 2A, lanes 10–15). Thus, the stability of *ACAD9* is independent of other known

components of the MCIA complex, while the stability of TMEM126B is highly dependent on the presence of the NDUFAF1, ECSIT, and ACAD9 (Figure 2B). Loss of TIMMDC1 did not lead to changes in the steady-state levels of any of the MCIA complex subunits, consistent with its role in the assembly of an independent complex I assembly module.

BN-PAGE and immunoblot analysis using antibodies against the complex I subunit NDUFA9 revealed that loss of any individual assembly factor led to the complete loss of mature complex I (Figure 2C). Furthermore, specificity of the genome editing was confirmed by complementation with the wild-type protein encoding a C-terminal FLAG epitope (Figure S1A), with a complete rescue of the complex I defect observed in each case (Figure 2C). Analysis of respiratory complexes III-V by BN-PAGE also showed normal levels relative to control mitochondria, with the only defect observed being the absence of the respirasome due to loss of complex I (Figures S1B–S1F). SDS-PAGE and immunoblot analysis revealed a consistent reduction in the levels of complex I subunits relative to control mitochondria, with the intermembrane space (IMS) localized NDUFS5 being the most strongly reduced subunit across all cell lines (Figure 2D). Strong decreases were also observed for ND1, NDUFA13, NDUFS3, and NDUFA9, whereas NDUFS2 and NDUFB6 were moderately decreased. Residual amounts of NDUFA13 and mtDNA-encoded ND1 were detected in the absence of NDUFAF1, ECSIT, ACAD9, and TMEM126B, but no signal was observed in the TIMMDC1<sup>KO</sup> cell lines (Figure 2D, compare ND1 and NDUFA13 lanes 1–12 to 13–15). These data support TIMMDC1 having a prominent role in the biogenesis of ND1 and/or associated proteins, while the MCIA complex functions at a different stage of complex I assembly (Andrews et al., 2013; Guerrero-Castillo et al., 2017).

The interdependency of NDUFAF1, ECSIT, ACAD9, and TMEM126B led us to question if the multi-membrane spanning TMEM126B acts as the membrane anchor for the peripheral MCIA complex subunits as previously proposed (Guarani et al., 2014). In control cells, alkali extraction liberated a portion of ACAD9, ECSIT, NDUFAF1, and cytochrome *c* into the supernatant fraction following ultracentrifugation (Figure 2E, lane 2), while the integral membrane proteins TMEM126B and NDUFB8 were present exclusively in the pellet fraction as expected (Figure 2E, lane 3). Following sonication treatment of control mitochondria, cytochrome *c* was extracted into the soluble fraction (Figure 2E, lane 4), while the remaining proteins were predominantly present in the pellet fraction (Figure 2E, lane 5), demonstrating their association with the inner membrane. Likewise, in TMEM126B<sup>KO</sup> mitochondria, ACAD9, ECSIT, and NDUFAF1 remained in the pellet fraction, similar to the membrane-embedded NDUFB8, while cytochrome *c* was extracted to the supernatant (Figure 2E, lanes 7 and 8). These data suggest that TMEM126B is not the exclusive membrane anchor of the MCIA complex.

### The MCIA Steady-State Complex Is Dependent on the Presence of Core ND2-Module Subunits

In order to gain insights into the behavior of the MCIA complex upon loss of the individual components, we investigated steady-state ACAD9-containing complexes. In mitochondria lacking NDUFAF1 or ECSIT, ACAD9 migrated only as a low mo-

lecular weight species (Figure 3A). In the TMEM126B<sup>KO</sup> and TIMMDC1<sup>KO</sup> cell lines, ACAD9 still formed high molecular weight complexes; however, these appeared to differ in abundance and distribution relative to control mitochondria. We suggest that these represent crippled complex I intermediates containing ACAD9. In contrast, analysis of TIMMDC1 complexes revealed the stable accumulation of the 400/440 kDa intermediates along with the presence of a higher molecular weight complex in all MCIA KO mitochondria (Figure 3B). Taken together, these results indicate that while all KOs ultimately result in a complex I defect, NDUFAF1, ECSIT, and ACAD9 are critical to forming all MCIA-dependent assembly intermediates, while loss of TMEM126B results in an altered assembly profile indicative of a perturbed assembly pathway.

Given the differences observed in subunit and assembly factor distribution in these KO cells, we sought to determine if there was a defect in the synthesis or stability of mtDNA-encoded subunits following pulse-chase labeling with [<sup>35</sup>S]-methionine (Formosa et al., 2016). In contrast to control cells, we observed turnover of ND2 in NDUFAF1<sup>KO</sup>, ECSIT<sup>KO</sup>, and ACAD9<sup>KO</sup> cell lines by 3 h post-chase and no signal detected by 24 h (Figure 3C, lanes 3–12). In TMEM126B<sup>KO</sup> cells, newly synthesized ND2 was present at all time points, suggesting that TMEM126B is not required for ND2 stability over the 24 h period (Figure 3C, lanes 13–15). TMEM126B showed reduced levels over the chase time following anisomycin treatment (Figure S2A), and this may be due to it being particularly labile under stress conditions (Fuhrmann et al., 2018; MacVicar et al., 2019).

In NDUFAF1<sup>KO</sup>, ECSIT<sup>KO</sup>, ACAD9<sup>KO</sup>, and TMEM126B<sup>KO</sup> cells, newly translated ND1 was initially similar to that observed in control cells (Figure 3C, compare lanes 1 with lanes 4, 7, 10, and 13), but was reduced at 3 h and 24 h time points (Figure 3C, lanes 4–15). This was consistent with previous findings that loss of ND2 promoted increased turnover of ND1 (Dunning et al., 2007). In the TIMMDC1<sup>KO</sup> cell line, ND2 was present and decreased in a similar manner to the control cells (Figure 3C, lanes 1–3 compared to lanes 16–18); however, the signal for ND1 was not detectable even directly following the pulse time point. This is consistent with TIMMDC1 involved in the biogenesis of ND1, while the MCIA complex is involved in the biogenesis of the ND2-module. Finally, it should be noted that the KO lines showed an apparent increased translation of non-complex I subunits in comparison to the control cell line. Because the steady-state levels of OXPHOS complexes are not increased in the knockout lines (Figure S1), the results suggest potential dysregulation of transcription or translation of mtDNA-encoded subunits.

Because the ND2-module harbors mtDNA-encoded subunits ND2, ND3, ND4L, and ND6, we investigated the interaction of NDUFAF1 and ECSIT with newly synthesized mtDNA-encoded subunits in further detail. Co-immunoprecipitation analysis revealed a strong interaction of both NDUFAF1 and ECSIT with ND2 and to a lesser extent with ND1, ND3, and ND4L, which decreased at 3 h post chase (Figure 3D, compare lanes 3 and 4 with lanes 6 and 7). After 24 h, where subunits have assembled into complex I, neither NDUFAF1 or ECSIT were found in association with mtDNA-encoded subunits (Figure 3D, lanes 9 and 10). Importantly, the pre-immune sera did not enrich any subunits (Figure 3D, lanes 2, 5, and 8). Given the relationship of the

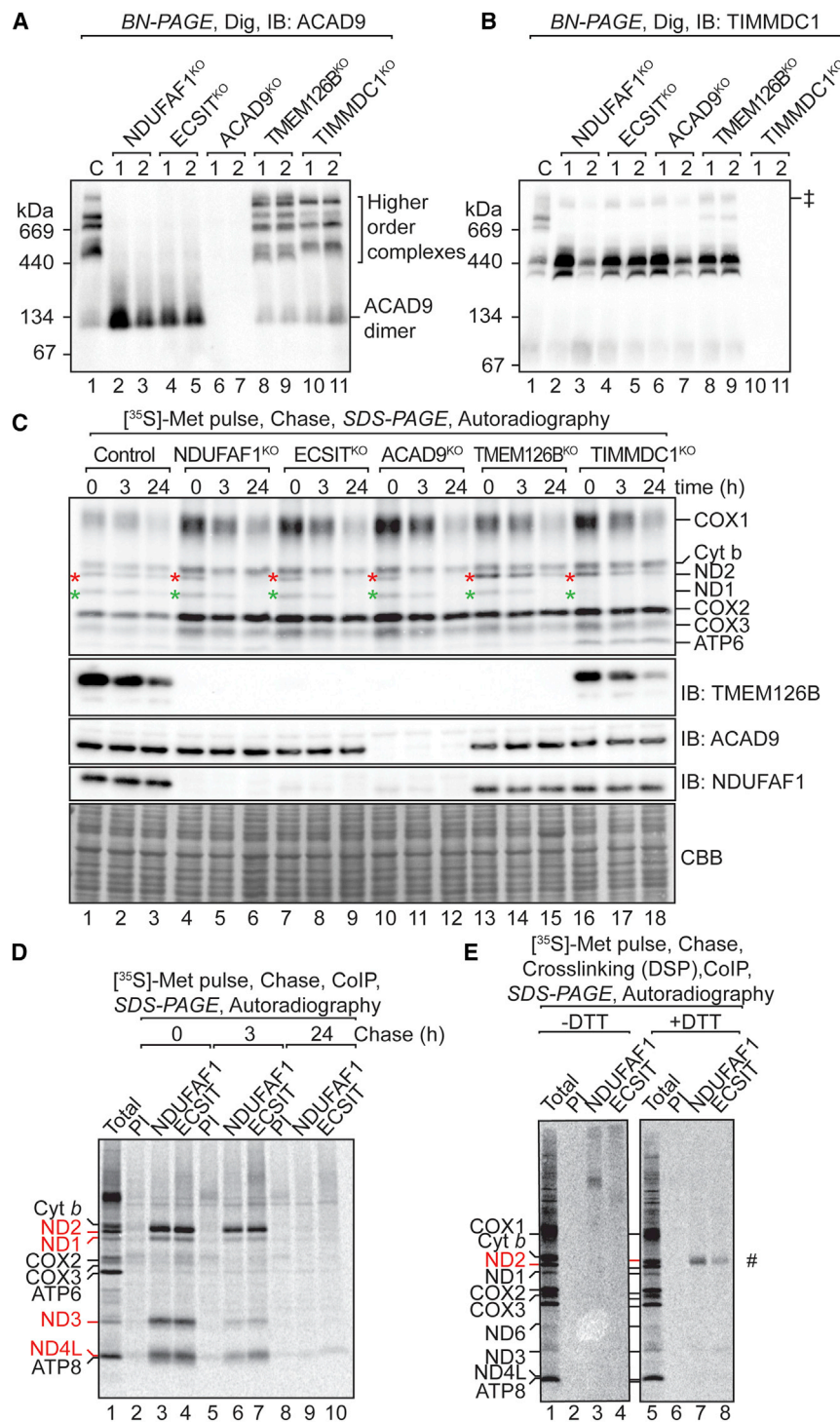


**Figure 3. Loss of the MCIA Complex Alters Complex I Assembly Intermediates**

(A and B) Mitochondria from indicated cell lines were solubilized in digitonin and analyzed by BN-PAGE and immunoblotting for (A) ACAD9 and (B) TIMMDC1.

(C) Cells were pulsed with  $[^{35}\text{S}]$ -Met for 2 h and chased for the indicated times. Isolated mitochondria were analyzed by SDS-PAGE and autoradiography. ND1, green asterisk; ND2, red asterisk. IB for TMEM126B, ACAD9 and NDUFAF1 served as controls. Coomassie Brilliant Blue (CBB) staining was indicative of loading.

(D) Following pulse chase labeling of 143B TK<sup>-</sup> cells, mitochondria were isolated and subjected to co-immunoprecipitation (coIP) using antibodies as indicated. Elutions were then subjected to SDS-PAGE and autoradiography.

(E) Samples (0 h) as described in (D) were subjected to chemical crosslinking using DSP, followed by coIP under denaturing conditions and analysis by SDS-PAGE under both reducing and non-reducing conditions and autoradiography. #, ND2.

See also Figure S2.

treatments showed indistinguishable phenotypes when analyzed by SDS-PAGE and BN-PAGE (Figure S2). We observed that NDUFAF1, ECSIT, and TMEM126B protein levels were reduced relative to their respective controls, as were the complex I subunits NDUFA13 and NDUFC2, while ACAD9 was largely unaffected (Figure S2B). Consistent with this, reduction of MCIA complexes was also observed (Figures S2C and S2D). These data suggest that the stability of the MCIA complex and its constituents is also dependent on the translation of associated mtDNA-encoded subunits. To differentiate between direct protein-protein interactions or associative interactions within a complex, chemical crosslinking using a thiol-cleavable crosslinker dithiobis-succinimidyl propionate (DSP) and co-immunoprecipitation was performed on mitochondrial lysates under denaturing conditions (Figure 3E). Following crosslinking under oxidizing conditions (-DTT), a clear radiolabeled species was observed in the NDUFAF1 elution samples that was absent in the pre-immune control (Figure 3E, lanes 2 and 3). Under reducing conditions where the crosslinker is cleaved (+DTT), the radiolabeled species observed following elution from NDUFAF1 antibodies was identified as ND2, which was also present after elution from ECSIT antibodies (Figure 3E, #). Taken together, these data suggest that while newly synthesized ND2 can be

MCIA complex with newly synthesized ND2, we sought to further investigate how mitochondrial translation inhibition affects the stability and assembly of this assembly complex. We analyzed 143B control ( $\rho^+$ ) and  $\rho^0$  cells, which lack mtDNA, as well as control HEK293T cells grown in the presence of chloramphenicol (CAP) to inhibit mitoribosome translation. Analysis of these two



translated independently of the MCIA complex, it directly contacts NDUFAF1 and ECSIT for further assembly. In the absence of these assembly factors, ND2 is unstable and degraded.

### Identification of TMEM186 as a Component of the MCIA Complex

It was reasoned that the ~450 kDa MCIA complex seen on BN-PAGE could not be fully accounted for by the molecular mass of the known protein constituents. We therefore utilized proximity-dependent biotin identification (BioID) (Roux et al., 2012) to identify proteins in proximity to the MCIA complex. NDUFAF1<sup>KO</sup> cells were rescued with NDUFAF1 fused to BirA\* (NDUFAF1<sup>BirA\*</sup>) and biotinylated proteins detected by quantitative mass spectrometry (Q-MS). All known components of the MCIA complex, as well as a number of complex I subunits were enriched in the NDUFAF1<sup>BirA\*</sup> sample (Figure 4A; Table S2). TMEM186, also significantly enriched in the NDUFAF1<sup>BirA\*</sup> sample, was recently found to co-migrate with components of the MCIA complex on BN-PAGE (Guerrero-Castillo et al., 2017). However, the importance of this protein in the assembly of complex I has not been addressed. *In vitro* import analysis revealed that TMEM186 contains a cleavable mitochondrial presequence and its import is dependent on the mitochondrial membrane potential (Figure 4B). TMEM186 is predicted to have two transmembrane anchors (Krogh et al., 2001). Indeed, TMEM186 with a C-terminal FLAG epitope (TMEM186<sup>FLAG</sup>) behaves like integral membrane protein Mic10 in alkali extraction studies, in contrast to peripheral membrane proteins NDUFAF1, NDUF2, and cytochrome c (Figure 4C). Furthermore, submitochondrial analysis using protease accessibility revealed that TMEM186<sup>FLAG</sup> was protected following outer membrane rupture, indicating that the C-terminal FLAG faces the matrix (Figure 4D). Matrix resident NDUFAF1 and NDUF2 were also protected from external protease following swelling, while the IMS-accessible protein Mic10 was only degraded following outer membrane rupture. As expected, the cytosolic exposed Mfn2 was degraded both with and without swelling (Figure 4D, lanes 2 and 4). Taken together, these data suggest that TMEM186 is inserted into the mitochondrial inner membrane, with both the N and C termini facing the matrix (Figure 4E).

We generated KO cell lines of TMEM186 (Table S1). Analysis of complex I from TMEM186<sup>KO</sup> cell lines by BN-PAGE showed only a modest decrease in levels—both in the supercomplex form (using digitonin solubilization) and holoenzyme form (using Triton X-100 solubilization) (Figure 4F). Analysis of the steady-state MCIA complexes revealed reduced levels and faster migration of the lowest MCIA complex that was rescued upon re-expression of TMEM186<sup>FLAG</sup> (Figures 4G and S3A, lanes 1–3). In contrast, TIMMDC1 complexes were unaffected (Figure S3A, lanes 4–6). Complexes III, IV, and V showed no striking differences in the steady-state levels between control and TMEM186<sup>KO</sup> mitochondria (Figure S3B). Furthermore, alkali extraction and sonication analysis of mitochondria isolated from control and TMEM186<sup>KO</sup> cells demonstrated that the peripheral membrane proteins NDUFAF1, ECSIT, and ACAD9 remained associated with the mitochondrial inner membrane, suggesting that TMEM186 was not required for the membrane association of the MCIA complex (Figure S3C).

In order to determine if TMEM186 is a constituent of the MCIA complex, we performed immuno-enrichment of TMEM186<sup>FLAG</sup> complexes using FLAG beads, followed by elution under native conditions and subsequent analysis by BN-PAGE (Figure 4H). Using mild digitonin solubilization, TMEM186<sup>FLAG</sup> was able to enrich the higher molecular weight ACAD9-containing complexes but not unassembled ACAD9 (Figure 4H). Under the more stringent, but still native conditions of Triton X-100 solubilization, TMEM186<sup>FLAG</sup> was only able to enrich the ~450 kDa complex, suggesting a stronger interaction with this assembly intermediate. The elutions were also subjected to Q-MS analysis for an unbiased overview of the protein interaction landscape. The digitonin solubilized TMEM186<sup>FLAG</sup> elutions revealed the significant enrichment of numerous proteins including a number of complex I subunits and assembly factors, as well as some subunits of respiratory complexes III and IV and the TIM22 translocase complex (Figure 4I, left panel; Table S3). The most highly enriched proteins were MCIA assembly factors NDUFAF1, ECSIT, and ACAD9, and to a lesser extent TMEM126B. In Triton X-100 eluates, TMEM186 specifically enriched NDUFAF1, ECSIT, and ACAD9 (Figure 4I, right panel; Table S4) whereas complex I, III, and IV subunits were not strongly enriched. TMEM186

### Figure 4. TMEM186 Is a Component of the MCIA Complex

- (A) BioID proximity labeling and protein enrichment in NDUFAF1<sup>BirA\*</sup> relative to control.  
 (B) *In vitro* import analysis of [<sup>35</sup>S]-TMEM186.  
 (C) Mitochondria from cells expressing TMEM186<sup>FLAG</sup> were subjected to alkali extraction (Na<sub>2</sub>CO<sub>3</sub>) followed by SDS-PAGE and immunoblot analysis.  
 (D) Mitochondria from cells expressing TMEM186<sup>FLAG</sup> were subjected to a swelling and protease protection assay followed by proteinase K incubation where indicated.  
 (E) Schematic representation of TMEM186 topology.  
 (F) Control and TMEM186<sup>KO</sup> mitochondria were solubilized in digitonin or Triton X-100, followed by BN-PAGE and immunoblotting with NDUFA9 antibodies. Complex II (SDHA) served as a loading control.  
 (G) Control, TMEM186<sup>KO</sup>, or rescue (TMEM186<sup>KO</sup>+TMEM186<sup>FLAG</sup>) mitochondria were solubilized in digitonin followed by BN-PAGE and immunoblotting with ACAD9 antibodies.  
 (H and I) Digitonin or Triton X-100 solubilized control or TMEM186<sup>KO</sup>+TMEM186<sup>FLAG</sup> mitochondria were subjected to affinity enrichment using FLAG agarose beads, followed by BN-PAGE analysis (H) and label-free quantitative proteomics (I).  
 (J) Following mtDNA-encoded subunit labeling, mitochondria were isolated and subjected to FLAG affinity enrichment. Eluates were analyzed by SDS-PAGE and phosphorimaging. Immunoblotting with FLAG and SDHA antibodies served as controls.  
 (K) Following CAP treatment, cells were chased and complex I *de novo* assembly analyzed by BN-PAGE. TOM40 served as a loading control. Right panel: Quantitation of NDUFA9 signal normalized to TOM40, all relative to untreated control (%). Error bars, n = 3, mean ± SEM. The asterisk (\*) indicates a non-specific band.

See also Figure S3 and Tables S1, S2, S3, and S4.



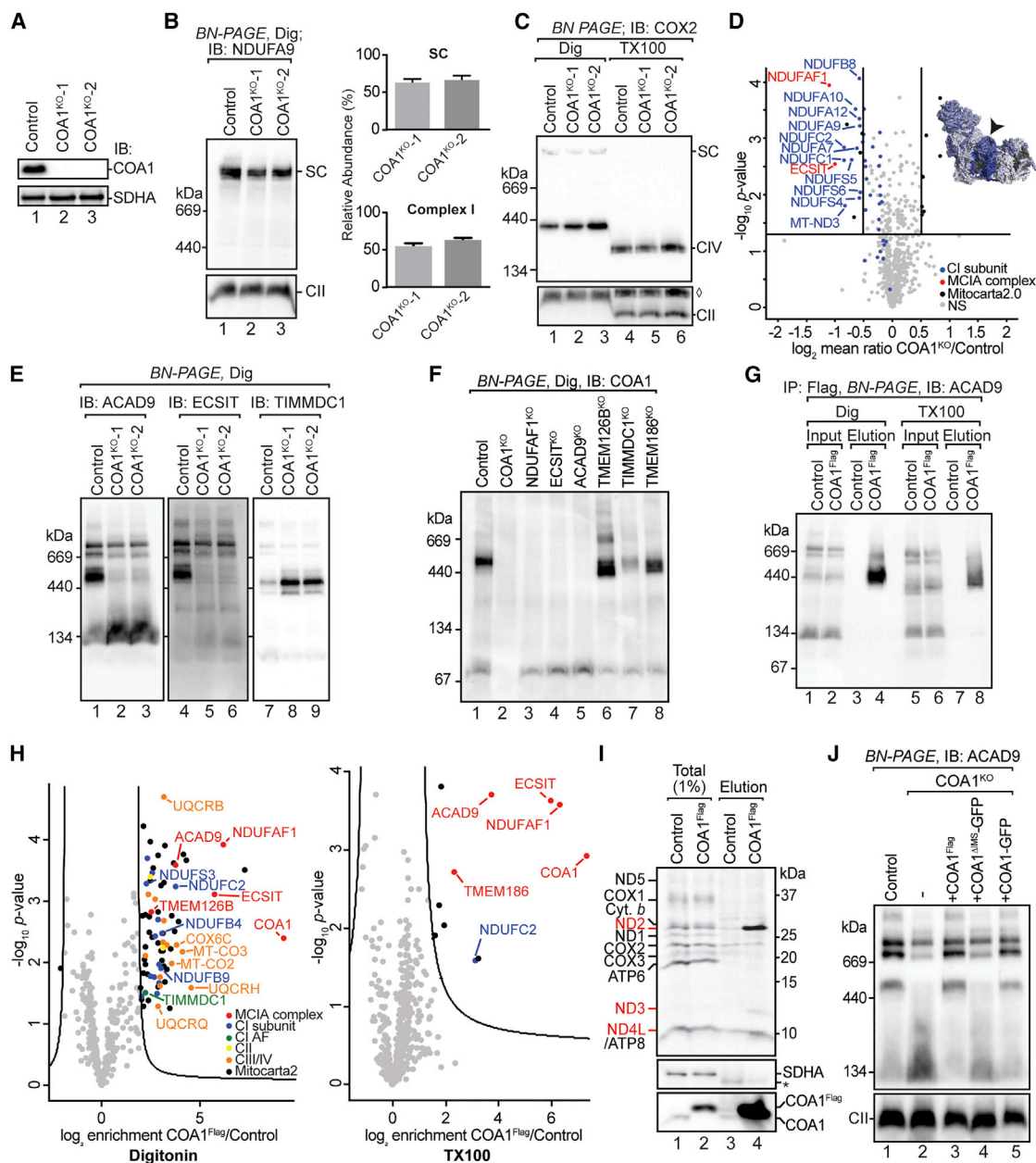


**Figure 5. COA1 Participates in Complex I Assembly and Is Required for MCIA Complex Stability**

(A) SDS-PAGE and immunoblot analysis of COA1 in mitochondria from control and COA1<sup>KO</sup> cells. SDHA is as a loading control.

(B) Digitonin solubilized mitochondria from control and COA1<sup>KO</sup> cells were subjected to BN-PAGE and immunoblotting using NDUFA9 antibodies. Complex II (SDHA) served as a loading control. Relative abundance to control supercomplex (SC) or complex I shown as mean  $\pm$  SEM, n = 3.

(C) Detergent solubilized mitochondria from control and COA1<sup>KO</sup> cells were subjected to BN-PAGE and immunoblotting using COX2 antibodies. Complex II (SDHA) served as a loading control. The diamond ( $\diamond$ ) indicates previous COX2 signal.

(D) Volcano plot showing proteins with altered abundance in COA1<sup>KO</sup> mitochondria. Inset: complex I subunit changes mapped onto the structure of complex I (PDB: 5LDW).

(E) Digitonin solubilized mitochondria from control and COA1<sup>KO</sup> cells were subjected to BN-PAGE and immunoblotting using antibodies directed to ACAD9, ECSIT, and TIMMDC1.

(F) Digitonin solubilized mitochondria from control and MCIA KO cells were subjected to BN-PAGE and immunoblotting using COA1 antibodies.

(G) Detergent solubilized mitochondria from control or COA1<sup>KO</sup>+COA1<sup>FLAG</sup> mitochondria were subjected to affinity enrichment using anti-FLAG agarose beads. Elutions were subjected to BN-PAGE and immunoblotting using ACAD9 antibodies.

(H) Samples were prepared as in (G) and subjected to LFQ proteomics.

(legend continued on next page)

was also enriched with the TIM22 import machinery (TIM22, TIM29, AGK, and small TIMs). The abundance and mobility of the TIM22 complex was not changed in TMEM186<sup>KO</sup> mitochondria (Figure S3D) suggesting that TMEM186 is not part of this machinery. *In vitro* import kinetics of TMEM186 into AGK<sup>KO</sup> mitochondria (Kang et al., 2017) appeared similar to control mitochondria, in contrast to the TIM22 substrate glutamate carrier (GC1) (Figure S3E), indicating that TMEM186 is not dependent on the TIM22 complex for its biogenesis. Given these findings, along with the presence of an N-terminal cleavable presequence that is typically seen for proteins imported via the TIM23-sorting pathway (Kang et al., 2018), the interaction between TMEM186 and the TIM22 machinery may be non-specific due to overexpression of the FLAG-tagged protein.

Next, control and TMEM186<sup>FLAG</sup>-expressing cells were pulse labeled with [<sup>35</sup>S]-methionine and subjected to co-immunoprecipitation using FLAG beads. As can be seen (Figure 4J), ND3 was the most enriched subunit under both digitonin and Triton X-100 solubilization conditions. TMEM186<sup>FLAG</sup> also specifically enriched ND2 and ND4L. We conclude that TMEM186, indeed, interacts with the core MCIA members NDUFAF1, ECSIT, and ACAD9, as part of the assembly of the ND2 module with a possible role in biogenesis of the ND3 subunit.

Because the loss of TMEM186 does not block complex I biogenesis, we investigated whether the rate of *de novo* complex I assembly was altered in the KO cells. Steady-state respiratory complexes were depleted from control, TMEM186<sup>KO</sup> clones, and rescue cell lines by CAP treatment for 96 h. CAP was then removed and *de novo* assembly of complex I analyzed (Figure 4K). In both TMEM186<sup>KO</sup> cell lines, the rate of complex I assembly was decreased to ~40% of control mitochondria, while this defect was rescued upon expression of TMEM186<sup>FLAG</sup> (Figure 4K). We conclude that, while TMEM186 is not an essential component of the complex I assembly machinery, loss of TMEM186 is refractory to the optimal function of the MCIA complex resulting in reduced assembly of complex I.

### COA1 Is Required for Complex I Assembly, but Dispensable for Complex IV Assembly

Guerrero-Castillo et al. (2017) recently proposed that the previously reported complex IV assembly factor COA1 (also known as MITRAC15) (Mick et al., 2012) may play a role in the biogenesis of complex I because it co-migrated on BN-PAGE with components of the MCIA complex and assembly intermediates. Consistent with this, we found that under mild conditions of digitonin solubilization, COA1 was also enriched with TMEM186<sup>FLAG</sup> (Figure 4I). The importance of COA1 in complex I assembly however, was not specifically addressed. We generated and validated COA1<sup>KO</sup> cells (Figure 5A; Table S1). BN-PAGE analysis revealed that complex I still assembled in the COA1<sup>KO</sup> cell lines but at an ~50% reduction in comparison to control mitochondria (Figure 5B). In contrast to previous reports using COA1 depletion by RNA interference (Mick et al., 2012), knockout of COA1 did

not appear to have an effect on complex IV levels (Figures 5C and S4A). No differences were observed in the levels of complex III (Figure S4B) or complex V (Figure S4C).

Stable isotope labeling by amino acids in cell culture (SILAC) and Q-MS analysis revealed reduced levels of NDUFAF1 and ECSIT in COA1<sup>KO</sup> mitochondria as well as complex I subunits belonging to the ND2-module (Figure 5D; Table S5), consistent with defects in the MCIA complex. This was recapitulated using SDS-PAGE and immunoblotting of mitochondria from control and COA1<sup>KO</sup> cells for various proteins (Figure S4D), showing decreased protein levels for TMEM126B (not quantified by Q-MS), ECSIT, and NDUFAF1, and complex I subunits NDUFC2 and NDUFS5. No changes to ACAD9, TIMMDC1, the complex I subunit NDUFS2, or complex IV subunits COX1 and COX4 were observed. We next addressed whether loss of COA1 affects the assembly or stability of the MCIA complex (Figure 5E). The ~450 kDa MCIA complex was specifically lost with the accumulation of free ACAD9 but not ECSIT (Figure 5E). Similar to what was observed for other MCIA KO cell lines, loss of COA1 also resulted in the accumulation of TIMMDC1 complexes containing the ND1/Q modules (Figure 5E). To further investigate how COA1 behaves with respect to the MCIA complex, we performed BN-PAGE using mitochondria from each of the MCIA complex KO lines (Figure 5F). In control cells, COA1 assembled in an ~450 kDa complex, which was absent in cells lacking NDUFAF1, ECSIT, or ACAD9, thus pointing to a direct and stable association of COA1 with this complex. Supporting this, COA1 migrated in the MCIA complexes that were altered in size or abundance in TMEM126B<sup>KO</sup>, TIMMDC1<sup>KO</sup>, and TMEM186<sup>KO</sup> mitochondria (Figure 5F). We conclude that COA1 is integral to the stabilization of the ~450 kDa MCIA complex.

Expression of COA1<sup>FLAG</sup> in COA1<sup>KO</sup> cells restored complex I (Figure S4E), ACAD9, and TIMMDC1 complexes back to control levels (Figure S4F). Co-immunoprecipitation analysis resulted in the enrichment of the ~450 kDa MCIA species (Figure 5G). Q-MS analysis of COA1<sup>FLAG</sup> elutions revealed that under mild digitonin conditions, COA1 highly enriched NDUFAF1, ECSIT, and ACAD9 along with a number of respiratory chain subunits from complexes I, III, and IV (Figure 5H, left panel; Table S6). Q-MS analysis of Triton X-100 solubilized mitochondria supported a stable interaction between COA1 and MCIA components ACAD9, ECSIT, NDUFAF1, and TMEM186 (Figure 5H, right panel; Table S7). In addition, NDUFC2, a complex I subunit belonging to the ND2-module (Fiedorczuk et al., 2016; Stroud et al., 2016) was also enriched. To investigate the possible interaction between COA1 and newly translated mtDNA-encoded subunits, we performed co-immunoprecipitation analysis of pulse-labeled mtDNA translation products. In this case, COA1 efficiently immunoprecipitated newly synthesized ND2, and to a lesser extent ND3 and ND4L (Figure 5I). Taken together, COA1 is a structural component of the MCIA complex and is critical to the formation and stability of the ~450 kDa assembly intermediate complex and the ND2-module.

(I) Pulse labeled mtDNA-encoded subunits from control or COA1<sup>KO</sup>+COA1<sup>FLAG</sup> cells were subjected to affinity enrichment and analysis by SDS-PAGE and phosphorimaging. Immunoblotting with COA1 and SDHA antibodies served as controls.

(J) Digitonin solubilized mitochondria were subjected to BN-PAGE and immunoblotting for ACAD9.

See also Figure S4 and Tables S1, S5, S6, and S7.

In comparison to other components of the MCIA complex, COA1 has an unusual topology, with only a small matrix facing polypeptide followed by a single transmembrane anchor and a “Tim21-family” domain facing the IMS (Mick et al., 2012). To determine if the IMS domain is required for COA1 function, we generated COA1<sup>KO</sup> cell lines expressing COA1 with either a C-terminal FLAG tag (COA1<sup>FLAG</sup>) or a GFP fusion (COA1-GFP), or with the IMS domain of COA1 substituted with GFP (COA1<sup>ΔIMS</sup>-GFP) (Figure S4G). Cells expressing COA1-GFP could restore assembly of ACAD9 complexes to the same degree as COA1<sup>FLAG</sup>, but loss of the IMS domain did not (Figure 5J). We conclude that, while topologically separated from the remaining components of the MCIA complex, the IMS domain of COA1 is important for the biogenesis of complex I through the stabilization of the ~450 kDa MCIA complex. These data suggest a prominent role of COA1 in the assembly of complex I through the MCIA complex.

## DISCUSSION

### Dissection of the MCIA Complex Components

The MCIA complex represents a key factor in the assembly of complex I and its importance has long been appreciated with analysis of both patient-derived fibroblasts as well as knock-down in cell culture (Dunning et al., 2007; Heide et al., 2012; Nouws et al., 2010; Vogel et al., 2005, 2007b). Furthermore, homologs of some MCIA complex assembly factors exist in most eukaryotes that harbor complex I (Chuaijit et al., 2019; Garcia et al., 2017; Küffner et al., 1998; Ligas et al., 2019). What has remained unclear is the interplay of the components of the MCIA complex and how they each may contribute to assembly.

Here, we found that deletion of each component individually leads to (1) different effects on MCIA complex subunit levels, (2) different steady-state levels of intermediate complexes, and (3) differences in the assembly kinetics of complex I. ACAD9 is required for the stability of all other components of the MCIA complex, while TMEM126B is not a requisite for stability of the remaining subunits of the assembly complex. Furthermore, while ACAD9 protein levels were unchanged upon loss of NDUFAF1 and ECSIT, both of these assembly factors are essential for ACAD9 to form higher molecular weight complexes. Taking into consideration the interconnected stability and effect on the assembly pathway, ACAD9-ECSIT-NDUFAF1 appear to form the “core” of the MCIA complex, while TMEM126B may engage more transiently. A number of observations lead to this conclusion. First, loss of TMEM126B does not preclude the formation of higher-order molecular weight complexes containing ACAD9, which are critically dependent on NDUFAF1 and ECSIT. Second, TMEM126B was not readily isolated with COA1 or TMEM186 under the harsher condition imposed by Triton X-100 solubilization, whereas NDUFAF1, ECSIT, and ACAD9 were consistently enriched. Finally, deletion of TMEM126B did not affect the stability of the remaining MCIA complex components, suggesting that they are capable of forming a stable complex. It should be noted that TMEM126B is still a critical component as its loss blocks complex I assembly. Indeed, modulation of TMEM126B levels may also be a mechanism for direct regulation of complex I levels, for example during chronic hypoxia (Fuhrmann et al., 2018).

### Assembly and Stability of the MCIA Complex Is Coupled to Translation

The MCIA complex is dependent on the expression of mtDNA-encoded proteins. TMEM126B, ECSIT, and NDUFAF1 levels were strongly reduced upon depletion of mtDNA or by inhibition of mitochondrial translation. The levels of ACAD9 were largely unaffected, consistent with its stoichiometric excess and potential role in beta-oxidation of fatty acids (Nouws et al., 2014). Assembly of the MCIA complex is stabilized by the presence of newly translated subunits—in particular that of ND2. This is supported by the direct interaction of ND2 with NDUFAF1 and ECSIT through chemical cross-linking as well as previous complexome studies into *de novo* complex I assembly (Guerrero-Castillo et al., 2017). Previous analysis of cells lacking the ND2-module accessory subunits NDUFC1 or NDUFC2 also did not show decreased levels of MCIA subunit proteins (Stroud et al., 2016), consistent with the observation of higher molecular-weight complexes containing ACAD9 in these cells.

### TMEM186 and COA1 Are MCIA Complex Subunits Required for Efficient Assembly of Complex I

We also demonstrated that TMEM186 and COA1 are MCIA components that play more peripheral functions to the core machinery. Until now, little was known regarding the role of TMEM186 other than an interaction with ECSIT (Guarani et al., 2014) and co-migration with the MCIA complex on BN-PAGE (Guerrero-Castillo et al., 2017). Loss of TMEM186 appears to affect the rate of *de novo* assembly of the enzyme. Furthermore, we observed a strong enrichment between TMEM186 and newly translated ND3 of the ND2-module. This is in agreement with the assembly model built based on complexome profiling suggesting that TMEM186 and ND3 enter the assembly pathway at the same stage (Guerrero-Castillo et al., 2017). The reduced kinetics of complex I assembly in TMEM186<sup>KO</sup> cells may be due to perturbed ND3 integration at this step.

In human cells, Mick et al. (2012) identified COA1 as a component of the MITRAC complex involved in the assembly or stability of the complex IV subunit COX1; however, a reduction in complex I levels was also shown upon COA1 knockdown. In addition, COA1 co-migrated with the MCIA complex and complex I intermediates on BN-PAGE (Guerrero-Castillo et al., 2017). Through KO approaches, we found that neither the level of assembled complex IV nor its constituent subunits were affected by deletion of COA1. Indeed, during the review of this manuscript, Wang et al. (2020) have clarified that human COA1 is indeed predominantly associated with the MCIA complex rather than in the MITRAC complexes. Nevertheless, it cannot be ruled out that deletion of COA1 may present differently in different tissues and a complex IV defect may be observed in a tissue-dependent context. Another interesting aspect of COA1 function is the peculiar topology this protein exhibits, where it contains an N-terminal transmembrane anchor with a TIM21-like domain that protrudes into the IMS (Mick et al., 2012). We found that the IMS domain is critical for the stability of the MCIA complex. So how does this domain, which is spatially segregated from the bulk of the MCIA complex, help in coordinating complex I assembly? The answer may lie in the strong interaction observed between newly synthesized ND2 and COA1. ND2 contains 10

transmembrane-spanning helices and needs to be carefully threaded into the membrane. Newly synthesized ND2 first accumulates in the ~450 kDa complex (Dunning et al., 2007; Lazarou et al., 2007) where it also cross-links with ECSIT and NDUFAF1. This complex was also strongly destabilized in the COA1<sup>KO</sup> cells. An interaction between COA1 and newly synthesized ND2 was also seen by Wang et al. (2020); however, it was suggested that COA1 works upstream of ACAD9 by promoting matrix-translation of ND2 as part of a ribosome-nascent chain complex. Given the topology of COA1, additional interacting matrix-facing proteins would be expected for such regulation. Future work into how COA1 functions mechanistically will be crucial to untangle the role of this protein.

## STAR★METHODS

Detailed methods are provided in the online version of this paper and include the following:

- KEY RESOURCES TABLE
- LEAD CONTACT AND MATERIALS AVAILABILITY
- EXPERIMENTAL MODEL AND SUBJECT DETAILS
- METHODS DETAILS
  - Cell culturing
  - Transfection and stable cell line generation
  - Gene editing and Screening
  - Mitochondrial isolation, gel electrophoresis, immunoblot analysis and antibodies
  - Proximity biotin identification (BioID)
  - Affinity enrichment
  - mtDNA- encoded protein metabolic labeling and *in vitro* protein import
  - Proteomics analysis
- QUANTIFICATION AND STATISTICAL ANALYSIS
- DATA AND CODE AVAILABILITY

## SUPPLEMENTAL INFORMATION

Supplemental Information can be found online at <https://doi.org/10.1016/j.celrep.2020.107541>.

## ACKNOWLEDGMENTS

We thank lab members for constructive discussions, the Bio21 Mass Spectrometry and Proteomics Facility (MMSPF), the Monash Proteomics and Metabolomics Facility (MPMF) for the provision of instrumentation, training, and technical support, and Monash Flowcore for cell sorting. T.D.J. is supported by an Australian Government Research Training Program (RTP) Scholarship. We acknowledge funding from the National Health and Medical Research Council (NHMRC project grants 1164459 to M.T.R., 1125390 and 1140906 to M.T.R. and D.A.S., and NHMRC Fellowship 1140851 to D.A.S.), a Research Fellowship from the Mito Foundation, and funding from the Australian Research Council (DP170101249 to D.S.).

## AUTHOR CONTRIBUTIONS

Conceptualization, L.E.F. and M.T.R.; Methodology, L.E.F., L.M.-W., B.R., A.J.S., M.L., D.S., D.A.S., and M.T.R.; Formal Analysis, L.E.F., B.R., D.A.S., and M.T.R.; Investigation, L.E.F., L.M.-W., B.R., A.J.S., T.D.J., and M.L.; Data Curation, L.E.F., B.R., D.A.S., and M.T.R.; Writing – Original Draft, L.E.F. and M.T.R.; Writing – Review & Editing, L.E.F., L.M.-W., B.R., A.J.S.,

T.H.B., M.L., D.A.S., and M.T.R.; Visualization, L.E.F. and M.T.R.; Supervision, D.A.S. and M.T.R.; Project Administration, M.T.R.; Funding Acquisition, D.A.S. and M.T.R.

## DECLARATION OF INTERESTS

The authors declare no competing interests.

Received: October 18, 2019

Revised: February 17, 2020

Accepted: March 27, 2020

Published: April 21, 2020

## REFERENCES

- Acín-Pérez, R., Bayona-Bafaluy, M.P.P., Fernández-Silva, P., Moreno-Loshuertos, R., Pérez-Martos, A., Bruno, C., Moraes, C.T., and Enriquez, J.A.A. (2004). Respiratory complex III is required to maintain complex I in mammalian mitochondria. *Mol. Cell* 13, 805–815.
- Acín-Pérez, R., Fernández-Silva, P., Peleato, M.L., Pérez-Martos, A., and Enriquez, J.A. (2008). Respiratory active mitochondrial supercomplexes. *Mol. Cell* 32, 529–539.
- Alston, C.L., Compton, A.G., Formosa, L.E., Strecker, V., Oláhová, M., Haack, T.B., Smet, J., Stouffs, K., Diakumis, P., Ciara, E., et al. (2016). Biallelic Mutations in TMEM126B Cause Severe Complex I Deficiency with a Variable Clinical Phenotype. *Am. J. Hum. Genet.* 99, 217–227.
- Andrews, B., Carroll, J., Ding, S., Fearnley, I.M., and Walker, J.E. (2013). Assembly factors for the membrane arm of human complex I. *Proc. Natl. Acad. Sci. USA* 110, 18934–18939.
- Bianchi, C., Genova, M.L., Parenti Castelli, G., and Lenaz, G. (2004). The mitochondrial respiratory chain is partially organized in a supercomplex assembly: kinetic evidence using flux control analysis. *J. Biol. Chem.* 279, 36562–36569.
- Calvo, S.E., Clauser, K.R., and Mootha, V.K. (2016). MitoCarta2.0: an updated inventory of mammalian mitochondrial proteins. *Nucleic Acids Res.* 44 (D1), D1251–D1257.
- Chuaijit, S., Boonyatistan, W., Boonchuay, P., Methetrairut, C., and Suthamarak, W. (2019). Identification of a novel mitochondrial complex I assembly factor ACDH-12 in *Caenorhabditis elegans*. *Mitochondrion* 46, 91–96.
- Dibley, M.G., Ryan, M.T., and Stroud, D.A. (2017). A novel isoform of the human mitochondrial complex I subunit NDUFV3. *FEBS Lett.* 591, 109–117.
- Dibley, M.G., Formosa, L.E., Lyu, B., Reljic, B., McGann, D., Muellner-Wong, L., Kraus, F., Sharpe, A.J., Stroud, D.A., and Ryan, M.T. (2020). The Mitochondrial Acyl-carrier Protein Interaction Network Highlights Important Roles for LYRM Family Members in Complex I and Mitochondrial Assembly. *Mol. Cell. Proteomics* 19, 65–77.
- Dunning, C.J., McKenzie, M., Sugiana, C., Lazarou, M., Silke, J., Connelly, A., Fletcher, J.M., Kirby, D.M., Thorburn, D.R., and Ryan, M.T. (2007). Human CIA30 is involved in the early assembly of mitochondrial complex I and mutations in its gene cause disease. *EMBO J.* 26, 3227–3237.
- Fassone, E., Taanman, J.-W.W., Hargreaves, I.P., Sebire, N.J., Cleary, M.A., Burch, M., and Rahman, S. (2011). Mutations in the mitochondrial complex I assembly factor NDUFAF1 cause fatal infantile hypertrophic cardiomyopathy. *J. Med. Genet.* 48, 691–697.
- Fedor, J.G., and Hirst, J. (2018). Mitochondrial Supercomplexes Do Not Enhance Catalysis by Quinone Channeling. *Cell Metab.* 28, 525–531.
- Fiedorczuk, K., Letts, J.A., Degliesposti, G., Kaszuba, K., Skehel, M., and Sazanov, L.A. (2016). Atomic structure of the entire mammalian mitochondrial complex I. *Nature* 538, 406–410.
- Formosa, L.E., Mimaki, M., Frazier, A.E., McKenzie, M., Stait, T.L., Thorburn, D.R., Stroud, D.A., and Ryan, M.T. (2015). Characterization of mitochondrial FOXRED1 in the assembly of respiratory chain complex I. *Hum. Mol. Genet.* 24, 2952–2965.
- Formosa, L.E., Hofer, A., Tischner, C., Wenz, T., and Ryan, M.T. (2016). Translation and Assembly of Radiolabeled Mitochondrial DNA-Encoded Protein

- Subunits from Cultured Cells and Isolated Mitochondria. *Methods Mol. Biol.* 1351, 115–129.
- Formosa, L.E., Dibley, M.G., Stroud, D.A., and Ryan, M.T. (2018). Building a complex complex: Assembly of mitochondrial respiratory chain complex I. *Semin. Cell Dev. Biol.* 76, 154–162.
- Fuhrmann, D.C., Wittig, I., Dröse, S., Schmid, T., Dehne, N., and Brüne, B. (2018). Degradation of the mitochondrial complex I assembly factor TMEM126B under chronic hypoxia. *Cell. Mol. Life Sci.* 75, 3051–3067.
- Garcia, C.J., Khajeh, J., Coulanges, E., Chen, E.I., and Owusu-Ansah, E. (2017). Regulation of Mitochondrial Complex I Biogenesis in *Drosophila* Flight Muscles. *Cell Rep.* 20, 264–278.
- Guarani, V., Paulo, J., Zhai, B., Huttlin, E.L., Gygi, S.P., and Harper, J.W. (2014). TIMMDC1/C3orf1 functions as a membrane-embedded mitochondrial complex I assembly factor through association with the MCIA complex. *Mol. Cell. Biol.* 34, 847–861.
- Guerrero-Castillo, S., Baertling, F., Kownatzki, D., Wessels, H.J., Arnold, S., Brandt, U., and Nijtmans, L. (2017). The Assembly Pathway of Mitochondrial Respiratory Chain Complex I. *Cell Metab.* 25, 128–139.
- Guo, R., Zong, S., Wu, M., Gu, J., and Yang, M. (2017). Architecture of Human Mitochondrial Respiratory Megacomplex I<sub>2</sub>III<sub>2</sub>IV<sub>2</sub>. *Cell* 170, 1247–1257.
- Haack, T.B., Danhauser, K., Haberberger, B., Hoser, J., Strecker, V., Boehm, D., Uziel, G., Lamantea, E., Invernizzi, F., Poulton, J., et al. (2010). Exome sequencing identifies ACAD9 mutations as a cause of complex I deficiency. *Nat. Genet.* 42, 1131–1134.
- Heide, H., Bleier, L., Steger, M., Ackermann, J., Dröse, S., Schwamb, B., Zörnig, M., Reichert, A.S., Koch, I., Wittig, I., and Brandt, U. (2012). Complexome profiling identifies TMEM126B as a component of the mitochondrial complex I assembly complex. *Cell Metab.* 16, 538–549.
- Hirst, J. (2013). Mitochondrial complex I. *Annu. Rev. Biochem.* 82, 551–575.
- Johnston, A.J., Hoogenraad, J., Dougan, D.A., Truscott, K.N., Yano, M., Mori, M., Hoogenraad, N.J., and Ryan, M.T. (2002). Insertion and assembly of human tom7 into the preprotein translocase complex of the outer mitochondrial membrane. *J. Biol. Chem.* 277, 42197–42204.
- Kang, Y., Stroud, D.A., Baker, M.J., De Souza, D.P., Frazier, A.E., Liem, M., Tull, D., Mathivanan, S., McConville, M.J., Thorburn, D.R., et al. (2017). Senegals Syndrome-Associated Mitochondrial Acylglycerol Kinase Is a Subunit of the Human TIM22 Protein Import Complex. *Mol. Cell* 67, 457–470.
- Kang, Y., Fielden, L.F., and Stojanovski, D. (2018). Mitochondrial protein transport in health and disease. *Semin. Cell Dev. Biol.* 76, 142–153.
- Kremer, L.S., Bader, D.M., Mertes, C., Kopajtich, R., Pichler, G., Iuso, A., Haack, T.B., Graf, E., Schwarzmayr, T., Terrile, C., et al. (2017). Genetic diagnosis of Mendelian disorders via RNA sequencing. *Nat. Commun.* 8, 15824.
- Krogh, A., Larsson, B., von Heijne, G., and Sonnhammer, E.L. (2001). Predicting transmembrane protein topology with a hidden Markov model: application to complete genomes. *J. Mol. Biol.* 305, 567–580.
- Küffner, R., Rohr, A., Schmiede, A., Krüll, C., and Schulte, U. (1998). Involvement of two novel chaperones in the assembly of mitochondrial NADH:Ubiquinone oxidoreductase (complex I). *J. Mol. Biol.* 283, 409–417.
- Kulak, N.A., Pichler, G., Paron, I., Nagaraj, N., and Mann, M. (2014). Minimal, encapsulated proteomic-sample processing applied to copy-number estimation in eukaryotic cells. *Nat. Methods* 11, 319–324.
- Lake, N.J., Formosa, L.E., Stroud, D.A., Ryan, M.T., Calvo, S.E., Mootha, V.K., Morar, B., Procopis, P.G., Christodoulou, J., Compton, A.G., and Thorburn, D.R. (2019). A patient with homozygous nonsense variants in two Leigh syndrome disease genes: Distinguishing a dual diagnosis from a hypomorphic protein-truncating variant. *Hum. Mutat.* 40, 893–898.
- Lapiente-Brun, E., Moreno-Loshuertos, R., Acín-Pérez, R., Latorre-Pellicer, A., Colás, C., Balsa, E., Perales-Clemente, E., Quirós, P.M., Calvo, E., Rodríguez-Hernández, M.A., et al. (2013). Supercomplex assembly determines electron flux in the mitochondrial electron transport chain. *Science* 340, 1567–1570.
- Lazarou, M., McKenzie, M., Ohtake, A., Thorburn, D.R., and Ryan, M.T. (2007). Analysis of the assembly profiles for mitochondrial- and nuclear-DNA-encoded subunits into complex I. *Mol. Cell. Biol.* 27, 4228–4237.
- Letts, J.A., Fiedorczuk, K., and Sazanov, L.A. (2016). The architecture of respiratory supercomplexes. *Nature* 537, 644–648.
- Letts, J.A., Fiedorczuk, K., Degliesposti, G., Skehel, M., and Sazanov, L.A. (2019). Structures of Respiratory Supercomplex I+III<sub>2</sub> Reveal Functional and Conformational Crosstalk. *Mol. Cell* 75, 1131–1146.
- Ligas, J., Pineau, E., Bock, R., Huynen, M.A., and Meyer, E.H. (2019). The assembly pathway of complex I in *Arabidopsis thaliana*. *Plant J.* 97, 447–459.
- Lim, S.C., Tajika, M., Shimura, M., Carey, K.T., Stroud, D.A., Murayama, K., Ohtake, A., and McKenzie, M. (2018). Loss of the Mitochondrial Fatty Acid  $\beta$ -Oxidation Protein Medium-Chain Acyl-Coenzyme A Dehydrogenase Disrupts Oxidative Phosphorylation Protein Complex Stability and Function. *Sci. Rep.* 8, 153.
- MacVicar, T., Ohba, Y., Nolte, H., Mayer, F.C., Tatsuta, T., Sprenger, H.-G., Lindner, B., Zhao, Y., Li, J., Bruns, C., et al. (2019). Lipid signalling drives proteolytic rewiring of mitochondria by YME1L. *Nature* 575, 361–365.
- McKenzie, M., Lazarou, M., Thorburn, D.R., and Ryan, M.T. (2007). Analysis of mitochondrial subunit assembly into respiratory chain complexes using Blue Native polyacrylamide gel electrophoresis. *Anal. Biochem.* 364, 128–137.
- Mick, D.U., Dennerlein, S., Wiese, H., Reinhold, R., Pacheu-Grau, D., Lorenzi, I., Sasarman, F., Weraarpachai, W., Shoubridge, E.A., Warscheid, B., and Rehling, P. (2012). MITRAC links mitochondrial protein translocation to respiratory-chain assembly and translational regulation. *Cell* 151, 1528–1541.
- Milenkovic, D., Blaza, J.N., Larsson, N.-G., and Hirst, J. (2017). The Enigma of the Respiratory Chain Supercomplex. *Cell Metab.* 25, 765–776.
- Montague, T.G., Cruz, J.M., Gagnon, J.A., Church, G.M., and Valen, E. (2014). CHOPCHOP: a CRISPR/Cas9 and TALEN web tool for genome editing. *Nucleic Acids Res.* 42, W401–7.
- Moreno-Lastres, D., Fontanesi, F., García-Consuegra, I., Martín, M.A., Arenas, J., Barrientos, A., and Ugalde, C. (2012). Mitochondrial complex I plays an essential role in human respirasome assembly. *Cell Metab.* 15, 324–335.
- Morgenstern, J.P., and Land, H. (1990). Advanced mammalian gene transfer: high titre retroviral vectors with multiple drug selection markers and a complementary helper-free packaging cell line. *Nucleic Acids Res.* 18, 3587–3596.
- Nouws, J., Nijtmans, L., Houten, S.M., van den Brand, M., Huynen, M., Venseelaar, H., Hoefs, S., Gloerich, J., Kronick, J., Hutchin, T., et al. (2010). Acyl-CoA dehydrogenase 9 is required for the biogenesis of oxidative phosphorylation complex I. *Cell Metab.* 12, 283–294.
- Nouws, J., Te Brinke, H., Nijtmans, L.G., and Houten, S.M. (2014). ACAD9, a complex I assembly factor with a moonlighting function in fatty acid oxidation deficiencies. *Hum. Mol. Genet.* 23, 1311–1319.
- Osellame, L.D., Singh, A.P., Stroud, D.A., Palmer, C.S., Stojanovski, D., Ramachandran, R., and Ryan, M.T. (2016). Cooperative and independent roles of the Drp1 adaptors Mff, MiD49 and MiD51 in mitochondrial fission. *J. Cell Sci.* 129, 2170–2181.
- Perales-Clemente, E., Fernández-Vizcarra, E., Acín-Pérez, R., Movilla, N., Bayona-Bafaluy, M.P., Moreno-Loshuertos, R., Pérez-Martos, A., Fernández-Silva, P., and Enríquez, J.A. (2010). Five entry points of the mitochondrially encoded subunits in mammalian complex I assembly. *Mol. Cell. Biol.* 30, 3038–3047.
- Perez-Riverol, Y., Csordas, A., Bai, J., Bernal-Llinares, M., Hewapathirana, S., Kundu, D.J., Inuganti, A., Griss, J., Mayer, G., Eisenacher, M., et al. (2019). The PRIDE database and related tools and resources in 2019: improving support for quantification data. *Nucleic Acids Res.* 47 (D1), D442–D450.
- Protasoni, M., Pérez-Pérez, R., Lobo-Jarne, T., Harbour, M.E., Ding, S., Peñas, A., Diaz, F., Moraes, C.T., Fearnley, I.M., Zeviani, M., et al. (2020). Respiratory supercomplexes act as a platform for complex III-mediated maturation of human mitochondrial complexes I and IV. *EMBO J.* 39, e102817.
- Pryde, K.R., Taanman, J.W., and Schapira, A.H. (2016). A LON-ClpP Proteolytic Axis Degrades Complex I to Extinguish ROS Production in Depolarized Mitochondria. *Cell Rep.* 17, 2522–2531.

- Puchades, C., Ding, B., Song, A., Wiseman, R.L., Lander, G.C., and Glynn, S.E. (2019). Unique Structural Features of the Mitochondrial AAA+ Protease AFG3L2 Reveal the Molecular Basis for Activity in Health and Disease. *Mol. Cell* 75, 1073–1085.
- Ran, F.A., Hsu, P.D., Wright, J., Agarwala, V., Scott, D.A., and Zhang, F. (2013). Genome engineering using the CRISPR-Cas9 system. *Nat. Protoc.* 8, 2281–2308.
- Rhein, V.F., Carroll, J., Ding, S., Fearnley, I.M., and Walker, J.E. (2013). NDUFAF7 methylates arginine 85 in the NDUFS2 subunit of human complex I. *J. Biol. Chem.* 288, 33016–33026.
- Rhein, V.F., Carroll, J., Ding, S., Fearnley, I.M., and Walker, J.E. (2016). NDUFAF5 Hydroxylates NDUFS7 at an Early Stage in the Assembly of Human Complex I. *J. Biol. Chem.* 291, 14851–14860.
- Roux, K.J., Kim, D.I., Raida, M., and Burke, B. (2012). A promiscuous biotin ligase fusion protein identifies proximal and interacting proteins in mammalian cells. *J. Cell Biol.* 196, 801–810.
- Ryan, M.T., Voos, W., and Pfanner, N. (2001). Assaying protein import into mitochondria. *Methods Cell Biol.* 65, 189–215.
- Sánchez-Caballero, L., Guerrero-Castillo, S., and Nijtmans, L. (2016a). Unraveling the complexity of mitochondrial complex I assembly: A dynamic process. *Biochim. Biophys. Acta* 1857, 980–990.
- Sánchez-Caballero, L., Ruzzenente, B., Bianchi, L., Assouline, Z., Barcia, G., Metodiev, M.D., Rio, M., Funalot, B., van den Brand, M.A.A., Guerrero-Castillo, S., et al. (2016b). Mutations in Complex I Assembly Factor TMEM126B Result in Muscle Weakness and Isolated Complex I Deficiency. *Am. J. Hum. Genet.* 99, 208–216.
- Sander, J.D., Maeder, M.L., Reyon, D., Voytas, D.F., Joung, J.K., and Dobbs, D. (2010). ZiFIT (Zinc Finger Targeter): an updated zinc finger engineering tool. *Nucleic Acids Res.* 38, W462–8.
- Sazanov, L.A. (2015). A giant molecular proton pump: structure and mechanism of respiratory complex I. *Nat. Rev. Mol. Cell Biol.* 16, 375–388.
- Schägger, H., and Pfeiffer, K. (2000). Supercomplexes in the respiratory chains of yeast and mammalian mitochondria. *EMBO J.* 19, 1777–1783.
- Schägger, H., and Pfeiffer, K. (2001). The ratio of oxidative phosphorylation complexes I–V in bovine heart mitochondria and the composition of respiratory chain supercomplexes. *J. Biol. Chem.* 276, 37861–37867.
- Schägger, H., and von Jagow, G. (1987). Tricine-sodium dodecyl sulfate-polyacrylamide gel electrophoresis for the separation of proteins in the range from 1 to 100 kDa. *Anal. Biochem.* 166, 368–379.
- Sheftel, A.D., Stehling, O., Pierik, A.J., Netz, D.J., Kerscher, S., Elsässer, H.P., Wittig, I., Balk, J., Brandt, U., and Lill, R. (2009). Human ind1, an iron-sulfur cluster assembly factor for respiratory complex I. *Mol. Cell. Biol.* 29, 6059–6073.
- Smith, A.C., and Robinson, A.J. (2019). MitoMiner v4.0: an updated database of mitochondrial localization evidence, phenotypes and diseases. *Nucleic Acids Res.* 47 (D1), D1225–D1228.
- Stiburek, L., Cesnekova, J., Kostkova, O., Fornuskova, D., Vinsova, K., Wenchich, L., Houstek, J., and Zeman, J. (2012). YME1L controls the accumulation of respiratory chain subunits and is required for apoptotic resistance, cristae morphogenesis, and cell proliferation. *Mol. Biol. Cell* 23, 1010–1023.
- Stroud, D.A., Maher, M.J., Lindau, C., Vögtle, F.N., Frazier, A.E., Surgenor, E., Mountford, H., Singh, A.P., Bonas, M., Oeljeklaus, S., et al. (2015). COA6 is a mitochondrial complex IV assembly factor critical for biogenesis of mtDNA-encoded COX2. *Hum. Mol. Genet.* 24, 5404–5415.
- Stroud, D.A., Surgenor, E.E., Formosa, L.E., Reljic, B., Frazier, A.E., Dibley, M.G., Osellame, L.D., Stait, T., Beilharz, T.H., Thorburn, D.R., et al. (2016). Accessory subunits are integral for assembly and function of human mitochondrial complex I. *Nature* 538, 123–126.
- Thompson, K., Mai, N., Oláhová, M., Scialó, F., Formosa, L.E., Stroud, D.A., Garrett, M., Lax, N.Z., Robertson, F.M., Jou, C., et al. (2018). OXA1L mutations cause mitochondrial encephalopathy and a combined oxidative phosphorylation defect. *EMBO Mol. Med.* 10, e9060.
- Trounce, I., Neill, S., and Wallace, D.C. (1994). Cytoplasmic transfer of the mtDNA nt 8993 T→G (ATP6) point mutation associated with Leigh syndrome into mtDNA-less cells demonstrates cosegregation with a decrease in state III respiration and ADP/O ratio. *Proc. Natl. Acad. Sci. USA* 91, 8334–8338.
- Tyanova, S., Temu, T., and Cox, J. (2016a). The MaxQuant computational platform for mass spectrometry-based shotgun proteomics. *Nat. Protoc.* 11, 2301–2319.
- Tyanova, S., Temu, T., Sinitcyn, P., Carlson, A., Hein, M.Y., Geiger, T., Mann, M., and Cox, J. (2016b). The Perseus computational platform for comprehensive analysis of (prote)omics data. *Nat. Methods* 13, 731–740.
- Ugalde, C., Vogel, R., Huijbens, R., Van Den Heuvel, B., Smeitink, J., and Nijtmans, L. (2004). Human mitochondrial complex I assembles through the combination of evolutionary conserved modules: a framework to interpret complex I deficiencies. *Hum. Mol. Genet.* 13, 2461–2472.
- Vogel, R.O., Janssen, R.J.R.J., Ugalde, C., Grovenstein, M., Huijbens, R.J., Visch, H.-J.J., van den Heuvel, L.P., Willems, P.H., Zeviani, M., Smeitink, J.A., and Nijtmans, L.G. (2005). Human mitochondrial complex I assembly is mediated by NDUFAF1. *FEBS J.* 272, 5317–5326.
- Vogel, R.O., Dieteren, C.E., van den Heuvel, L.P., Willems, P.H., Smeitink, J.A., Koopman, W.J., and Nijtmans, L.G. (2007a). Identification of mitochondrial complex I assembly intermediates by tracing tagged NDUFS3 demonstrates the entry point of mitochondrial subunits. *J. Biol. Chem.* 282, 7582–7590.
- Vogel, R.O., Janssen, R.J.R.J., van den Brand, M.A.A., Dieteren, C.E., Verkaart, S., Koopman, W.J., Willems, P.H., Pluk, W., van den Heuvel, L.P., Smeitink, J.A., and Nijtmans, L.G. (2007b). Cytosolic signaling protein Ecsit also localizes to mitochondria where it interacts with chaperone NDUFAF1 and functions in complex I assembly. *Genes Dev.* 21, 615–624.
- Wang, C., Richter-Dennerlein, R., Pacheu-Grau, D., Liu, F., Zhu, Y., Dennerlein, S., and Rehling, P. (2020). MITRAC15/COA1 promotes mitochondrial translation in a ND2 ribosome-nascent chain complex. *EMBO Rep.* 21, e48833.
- Wittig, I., Braun, H.-P.P., and Schägger, H. (2006). Blue native PAGE. *Nat. Protoc.* 1, 418–428.
- Zhu, J., Vinothkumar, K.R., and Hirst, J. (2016). Structure of mammalian respiratory complex I. *Nature* 536, 354–358.
- Zurita Rendón, O., and Shoubridge, E.A. (2012). Early complex I assembly defects result in rapid turnover of the ND1 subunit. *Hum. Mol. Genet.* 21, 3815–3824.
- Zurita Rendón, O., Silva Neiva, L., Sasarman, F., and Shoubridge, E.A. (2014). The arginine methyltransferase NDUFAF7 is essential for complex I assembly and early vertebrate embryogenesis. *Hum. Mol. Genet.* 23, 5159–5170.

## STAR★METHODS

### KEY RESOURCES TABLE

REAGENT or RESOURCE	SOURCE	IDENTIFIER
<b>Antibodies</b>		
Anti-ATP5A (IB: 1/1000)	Abcam	Cat# ab14748, RRID: AB_301447
Anti-COA1 (IB: 1/500)	Sigma-Aldrich	Cat# HPA011944, RRID: AB_1848671
Anti-Core 1 (IB: 1/1000)	ThermoFisher	Cat# 459140, RRID: AB_2532227
Anti-COX1 (IB: 1/1000)	ThermoFisher	Cat# 459600, RRID: AB_2532240
Anti-COX2 (IB: 1/1000)	ThermoFisher	Cat# A-6404, RRID: AB_221584
Anti-COX4 (IB: 1/1000)	Abcam	Cat# ab110261, RRID: AB_10862101
Anti-Cytochrome c (IB: 1/500)	BD labs	Cat# 556433, RRID: AB_396417
Anti-Flag M2 clone (IB: 1/1000)	Sigma-Aldrich	Cat# F1804, RRID: AB_262044
Anti-Mic10 (IB: 1/1000)	Aviva Systems Biology	Cat# ARP44801_P050, RRID: AB_2045181
Anti-NDUFA13 (IB: 1/1000)	Abcam	Cat# ab110240, RRID: AB_10863178
Anti-NDUFB8 (IB: 1/1000)	Abcam	Cat# ab110242, RRID: AB_10859122
Anti-NDUFC2 (IB: 1/1000)	Santa Cruz	Cat# sc-398719
Anti-NDUFS2 (IB: 1/1000)	Abcam	Cat# ab110249, RRID: AB_10861985
Anti-NDUFS3 (IB: 1/1000)	Innovative Research	Cat# A21343, RRID: AB_1501824
Anti-SDHA (IB: 1/1000)	Abcam	Cat# ab14715, RRID: AB_301433
Anti-TIM29 (IB: 1/1000)	Sigma-Aldrich	Cat# HPA041858, RRID: AB_10963429
Anti-TIMMDC1 (IB: 1/500)	Sigma-Aldrich	Cat# HPA053214, RRID: AB_2682081
Anti-TMEM126B (IB: 1/500)	Sigma-Aldrich	Cat# HPA014480, RRID: AB_1858083
Anti-TOM20 (IB: 1/1000)	Santa Cruz	Cat# sc-11415, RRID: AB_2207533
Anti-ACAD9 (IB: 1/500)	In house	N/A
Anti-ECSIT (IB: 1/500)	In house	N/A
Anti-Mfn2 (IB: 1/500)	In house	N/A
Anti-mtHSP70 (IB: 1/500)	In house	N/A
Anti-NDUFA9 (IB: 1/500)	In house	N/A
Anti-NDUFAF1 (IB: 1/500)	In house	N/A
Anti-NDUFB6 (IB: 1/500)	In house	N/A
Anti-NDUFS5 (IB: 1/500)	In house	N/A
Anti-ND1 (IB: 1/500)	Gift from A. Lombes (Paris)	N/A
Anti-TOM40 (IB: 1/500)	Gift from M. Mori (Kumamoto)	N/A
<b>Chemicals, Peptides, and Recombinant Proteins</b>		
Anisomycin	Sigma-Aldrich	A9789
EXPRE <sup>35S</sup> Protein Labeling Mix, [ <sup>35</sup> S]-, 7mCi (74MBq), 50mM Tricine (pH 7.4), 10mM 2-mercaptoethanol	Perkin Elmer	NEG072007MC
Puromycin	InvivoGen	ant-pr-1
Carbonyl cyanide 3'-chlorophenylhydrazone	Sigma-Aldrich	C2759
Anti-Flag M2 Affinity gel	Sigma-Aldrich	A2220
Flag peptide	Sigma-Aldrich	F3290
Digitonin- High purity	Merck	300410
Dithiobis(succinimidyl propionate)	Pierce	22585
Streptavidin magnetic beads	ThermoFisher	88816
Biotin	Sigma-Aldrich	B4639
Chloramphenicol	Sigma-Aldrich	C0378

(Continued on next page)

<b>Continued</b>		
REAGENT or RESOURCE	SOURCE	IDENTIFIER
Proteinase K, from <i>Tritirachium album</i>	Sigma-Aldrich	P6556
Deposited Data		
Raw MS data on PRIDE	This paper	PRIDE: PXD018075
Experimental Models: Cell Lines		
HEK293T cells	ATCC	CRL-3216
143B TK- osteosarcoma cells	<a href="#">Trounce et al., 1994</a>	N/A
143B TK- $\rho^0$ osteosarcoma cells	<a href="#">Trounce et al., 1994</a>	N/A
Flp-In T-REx HEK293 cells	ThermoFisher Scientific	Cat#: R75007; RRID: CVCL_U427
Flp-In T-REx HEK293 AGK <sup>KO</sup> cells	<a href="#">Kang et al., 2017</a>	N/A
Recombinant DNA		
pBABE-NDUF <sup>1</sup> Flag	This paper	N/A
pBABE-NDUF <sup>1</sup> BirA	This paper	N/A
pBABE-ECSIT <sup>1</sup> Flag	This paper	N/A
pBABE-ACAD9 <sup>1</sup> Flag	This paper	N/A
pBABE-TMEM126B <sup>1</sup> Flag	This paper	N/A
pBABE-TIMMDC1 <sup>1</sup> Flag	This paper	N/A
pBABE-TMEM186 <sup>1</sup> Flag	This paper	N/A
pLVX-COA1 <sup>1</sup> Flag	This paper	N/A
pLVX-COA1-GFP <sup>1</sup> Flag	This paper	N/A
pLVX-COA1 <sup>1</sup> $\Delta$ IMS-GFP <sup>1</sup> Flag	This paper	N/A
Software and Algorithms		
Image Lab software	Bio-Rad	RRID: SCR_003070
Prism v7	GraphPad	RRID: SCR_002798
MaxQuant Platform	<a href="#">Tyanova et al., 2016a</a>	RRID: SCR_014485
Perseus Platform	<a href="#">Tyanova et al., 2016b</a>	RRID:SCR_015753

## LEAD CONTACT AND MATERIALS AVAILABILITY

Further information and requests for reagents should be directed to, and will be fulfilled by the Lead Contact, Michael Ryan ([Michael.Ryan@monash.edu](mailto:Michael.Ryan@monash.edu)). All unique/stable reagents generated in this study are available from the Lead Contact with a completed Materials Transfer Agreement.

## EXPERIMENTAL MODEL AND SUBJECT DETAILS

Human epithelial kidney cells containing the SV40 T-antigen (HEK293T) were originally purchased from the ATCC and a clonal cell line was obtained after single cell sorting and used as the parental line for all gene editing and proteomic work ([Stroud et al., 2016](#)). Human 143B TK<sup>-</sup> osteosarcoma cell lines ( $\rho^+$  and  $\rho^0$ ) were obtained from I. Trounce ([Trounce et al., 1994](#)).

## METHODS DETAILS

### Cell culturing

Cells were cultured in DMEM supplemented with 10% (v/v) fetal bovine serum (FBS), 1 × penicillin/ streptomycin (Sigma-Aldrich; P4458), 1 × Glutamax (Life Technologies; 35050061) and 50 $\mu$ g/mL Uridine (Sigma-Aldrich; U3750). Cells were grown at 37°C with a 5% CO<sub>2</sub> atmosphere. Galactose containing DMEM was prepared from Glucose-free DMEM (Life Technologies; 11966-025) supplemented with 10% (v/v) dialysed FBS, 25mM D-galactose (Sigma-Aldrich; G0750), 1 × penicillin/ streptomycin (Sigma-Aldrich; P4458), 1 × Glutamax (Life Technologies; 35050-061), 1 × Sodium Pyruvate (Life Technologies; 11360-070) and 50 $\mu$ g/mL Uridine (Sigma-Aldrich; U3750).

For the chloramphenicol (CAP) and chase experiment, cells were grown for 4 days in glucose containing DMEM supplemented with 50 $\mu$ g/mL CAP to inhibit mtDNA encoded protein synthesis and deplete respiratory chain complexes. Efficiency was verified by the lack of cell growth on galactose-DMEM. For the chase, cells were then plated onto 10cm plates and regular culture media was added. Cells were harvested at the desired time points. Mitochondria were then isolated and analyzed by BN-PAGE.



For SILAC culture, cells were grown as previously described (Stroud et al., 2016). Briefly, cells were grown in DMEM without Lysine/Arginine (Assay Matrix; D9803-07B) supplemented with 10% (v/v) dialyzed FBS (GE Healthcare; SH30079.03), 1 × penicillin/ streptomycin (Sigma-Aldrich; P4458), 1 × Glutamax (Life Technologies; 35050061), 1 × Sodium Pyruvate (Life Technologies; 11360070) and 50 μg/mL Uridine (Sigma-Aldrich; U3750) and either ‘heavy’ amino acids ( $^{13}\text{C}_6$  $^{15}\text{N}_4$ -Arginine; Cambridge Isotope Labs Inc; CNLM-539-H-1,  $^{13}\text{C}_6$  $^{15}\text{N}_2$ -Lysine; Silantes; 211604102) or ‘light’ amino acids (Arginine; Sigma-Aldrich; A5131, Lysine; Sigma-Aldrich; L5626).

### Transfection and stable cell line generation

Cells were transfected using Lipofectamine LTX (Life Technologies; 15338100) according to manufacturer’s instructions. Stable, constitutive expression was achieved by transfecting HEK293T cells with pBABE-puro (Addgene; 1764) (Morgenstern and Land, 1990) encoding the cDNA of interest. Stable, inducible expression was achieved by transfecting cells with pLVX-TetOne-Puro (Clontech; 631849) encoding the cDNA of interest. All plasmids were sequence verified by Micromon (Monash University) or the Garvan Institute for Medical Research. Viral supernatants were collected after 48 hours and used to infect the corresponding KO cell lines. Cell lines were then selected by growth on galactose-containing DMEM, with the exception of TMEM186 and COA1 knockouts, which were selected for by the addition of 2 μg/mL puromycin. Expression was verified by BN-PAGE or SDS-PAGE as required.

### Gene editing and Screening

Gene editing was performed using TALEN pairs as described (Formosa et al., 2015) or the pSp-CAS9(BB)-2A-GFP (PX458) CRISPR/Cas9 construct (a gift from F. Zhang; Addgene plasmid 48138) (Ran et al., 2013). TALEN pairs were designed using ZiFIT Targeter (Sander et al., 2010) and CRISPR/Cas9 guide RNAs were designed using CHOPCHOP (Montague et al., 2014). KO cell lines for NDUFAF1 and TIMMDC1 have been previously reported (Lake et al., 2019; Stroud et al., 2016). Target sequences, gene disruption strategies and generated indels can be found in Table S1.

### Mitochondrial isolation, gel electrophoresis, immunoblot analysis and antibodies

Mitochondria were isolated as previously described (Johnston et al., 2002). Briefly, pelleted cells were resuspended in Isolation Buffer A (20 mM HEPES-KOH pH 7.6, 220 mM mannitol, 70 mM sucrose, 1 mM EDTA, 0.5 mM PMSF and 2 mg/mL BSA) and lysed with 20 strokes using a Dounce glass homogenizer. Lysed cells were centrifuged at 800 g to pellet nuclei and intact cells. Supernatants containing mitochondria were then centrifuged at 12,000 g for 10 minutes. The mitochondrial pellet was washed by resuspending in Isolation Buffer B (20 mM HEPES-KOH, 220 mM mannitol, 70 mM sucrose, 1 mM EDTA and 0.5 mM PMSF) and re-isolated by centrifugation at 12,000 g as above. Protein concentration was determined by bicinchoninic acid assay (BCA; Thermo Fisher Scientific; 23223). Mitochondria were used immediately or aliquoted and frozen at  $-80^\circ\text{C}$  until required. Membrane association and protease protection assay were performed as previously described (Ryan et al., 2001). For membrane association analysis, mitochondria were resuspended in sonication buffer (10 mM Tris pH 7.4, 100 mM NaCl) or alkali extraction buffer (100 mM  $\text{Na}_2\text{CO}_3$  pH 11.5–12) and incubated on ice for 30 minutes. Sonication was then performed on the appropriate samples on ice. To separate the membrane and soluble fractions, samples were subjected to ultracentrifugation at 100,000 g for 30 minutes. For sub-mitochondrial fractionation analysis, mitochondria were resuspended in isotonic buffer (10 mM MOPS pH 7.2, 250 mM sucrose) or hypotonic buffer (10 mM MOPS pH 7.2) to rupture the outer membrane, followed by the addition 50 μg/mL Proteinase K on ice as required. Proteinase K was inactivated by the addition of 1 mM PMSF on ice. All samples were then subjected to trichloroacetic acid (TCA) precipitation and then resuspended in loading dye for SDS-PAGE and immunoblotting analysis.

Tris-tricine SDS-PAGE and BN-PAGE were performed as previously described (McKenzie et al., 2007; Schagger and von Jagow, 1987; Wittig et al., 2006). For Tris-tricine SDS-PAGE, 10% acrylamide/bis-acrylamide solution made in tricine gel buffer (1M Tris pH 8.45, 0.1% (w/v) SDS) was used for the separating gel. The stacking gel was made with 4% acrylamide/bis-acrylamide in tricine gel buffer. Electrophoresis was performed using cathode buffer (0.1 M Tris, 0.1 M Tricine pH 7.4, 0.1% (w/v) SDS) and anode buffer (0.2 M Tris pH 8.9). For BN-PAGE, continuous 4%–13% gels were made using a gradient mixer. The separating gel was made with acrylamide/bis-acrylamide solutions that were made in BN gel buffer (66 mM  $\epsilon$ -amino n-caproic acid, 50 mM Bis-Tris pH 7.0) with 13% acrylamide/bis-acrylamide and 20% (w/v) glycerol or 4% acrylamide/bis-acrylamide alone. The stacker gel was composed of 4% acrylamide/bis-acrylamide in BN-gel buffer and layered onto the separating gel. Mitochondria were solubilised in detergent buffer (20 mM Bis-Tris pH 7.0, 50 mM NaCl, 10% (w/v) glycerol) containing 1% digitonin or 1% Triton X-100 for 10 minutes on ice, followed by centrifugation at 20,000 g for 10 minutes. The clarified supernatant containing mitochondrial complexes was then transferred to a clean tube containing one-tenth of the volume of 10x BN-PAGE loading dye (5% (w/v) Coomassie blue G250, 500 mM  $\epsilon$ -amino n-caproic acid, 100 mM Bis-Tris pH 7.0) before loading onto the gel. Electrophoresis was performed using BN-PAGE blue cathode buffer (50 mM tricine, 15 mM Bis-Tris, 0.02% (w/v) Coomassie blue G250), which was replaced with BN-PAGE clear cathode buffer (50 mM tricine, 15 mM Bis-Tris) after the dye front migrated half-way through the gel and BN-PAGE anode buffer (50 mM Bis-Tris pH 7.0). Following electrophoresis, transfer onto PVDF membrane (Merck; IPVH00010) was performed using a Novex Semi-Dry Blotter (Thermo Fisher) or an Invitrogen Power Blotter System (Thermo Fisher) according to manufacturer’s instructions. Primary antibodies, sources and associated dilutions are listed in the key resource table above. Anti-mouse (Sigma-Aldrich; A9044) or anti-rabbit (Sigma-Aldrich; A0545) horseradish peroxidase-conjugated secondary antibodies were used at a dilution of 1:10,000. Clarity western ECL chemiluminescent substrate (BioRad; 1705061) was used for detection on a BioRad ChemiDoc XRS+ imaging system according to the manufacturer’s instructions.

### Proximity biotin identification (BioID)

Biotin labeling and identification was performed as previously described with some modifications (Osellame et al., 2016; Roux et al., 2012). Briefly, NDUFAF1<sup>KO</sup> cells expressing NDUFAF1<sup>BirA\*</sup> or NDUFAF1<sup>HA</sup> were grown in standard DMEM supplemented with 50  $\mu$ M Biotin for 24 hours. Isolated mitochondria were solubilized in RIPA buffer (50 mM Tris-HCl pH 7.5, 150 mM NaCl, 1% NP-40, 1 mM EDTA, 1 mM EGTA and 0.1% SDS), supplemented with 1  $\times$  protease cocktail inhibitor (Sigma-Aldrich; 11873580001), 0.5% sodium deoxycholate and 250 U/mL benzonase (Sigma-Aldrich; E1014) and biotinylated proteins were enriched using streptavidin-coated magnetic beads (ThermoFischer; 88816). On-bead tryptic digest was performed using 5  $\mu$ g/mL mass spectrometry grade trypsin (Promega; V5113) overnight at 37°C with agitation. The beads were rinsed twice with mass spectrometry grade water, the rinse fraction was pooled with tryptic digests and peptides were then concentrated using vacuum centrifugation. The resulting pellets were resuspended in 0.1% TFA, 2% ACN prior to analysis by LC-coupled mass-spectrometry.

### Affinity enrichment

For affinity enrichment of Flag-tagged proteins, mitochondria from control or Flag-expressing cells were isolated and solubilized in 1% (w/v) digitonin or 1% (v/v) Triton X-100 in solubilization buffer (20mM Bis-Tris (pH 7.0), 50 mM NaCl, 10% (v/v) glycerol). Following clarification of lysates by centrifugation (16,000 g, 10 mins, 4°C), supernatants were applied to Flag affinity gel (Sigma) and incubated for 2 hours at 4°C with gentle rotation. Affinity gel was washed with 0.1% digitonin or 0.1% Triton X-100 in solubilization buffer as required. Proteins were eluted using 150  $\mu$ g/mL Flag peptide in solubilization buffer with 0.1% (w/v) digitonin or 0.1% (v/v) Triton X-100 as required. Samples were then prepared for BN-PAGE or proteomics analysis as described.

### mtDNA- encoded protein metabolic labeling and *in vitro* protein import

Radiolabelling of mtDNA-encoded proteins was performed using 10  $\mu$ g/mL Anisomycin (Sigma-Aldrich; A9789) to block cytosolic translation as previously described (Formosa et al., 2016). Isolated mitochondria were subjected to Flag affinity enrichment and/or SDS-PAGE analysis, followed by transfer to PVDF membrane and analyzed by phosphorimaging digital autoradiography (GE Healthcare).

For affinity enrichment of newly translated proteins, mitochondria were isolated after 2 hours of labeling with [<sup>35</sup>S]-Methionine/Cysteine mix and affinity enrichment performed as above. Bound proteins were removed from beads by incubating affinity gel in LDS sample buffer (Thermo Fisher; NP0008) with 100 mM DTT at room temperature for 15 minutes. Affinity gel was removed by centrifugation and proteins analyzed by Tris-Tricine SDS-PAGE as described above.

For co-immunoprecipitation of endogenous NDUFAF1 or ECSIT, 143B TK<sup>-</sup> osteosarcoma cells were labeled for 2 hours with [<sup>35</sup>S]-Methionine/Cysteine mix and chased for 0, 3 and 24 hours in DMEM. Isolated mitochondria were solubilized in 1% Triton X-100 and incubated with Protein A Sepharose crosslinked to pre-immune sera or NDUFAF1/ECSIT reactive sera. To determine direct protein-protein interactions, samples were initially incubated with 0.2 mM DSP in SM buffer (250 mM sucrose, 10 mM MOPS pH 7.2) followed by solubilization in 1% Triton X-100 and 1% SDS. Protein-antibody complexes were washed, and bound proteins were eluted in 100 mM Glycine pH 2.0 and prepared for SDS-PAGE with or without 100 mM DTT as indicated.

For *in vitro* protein import, the cDNA sequence of TMEM186 was amplified to incorporate a T7 promoter sequence (5'-GTACCG TAATACGACTCACTATAG-3') upstream of the initiation codon and a reverse primer to incorporate a poly-A tail (5'-T<sub>18</sub>CACTTGAG CATCTGATGTACCC-3'). Radiolabeled protein was generated using the TNT-T7 quick-coupled transcription/translation system (Promega; L1170). Alternatively, the TMEM186 and GC1 open reading frames were used as templates for *in vitro* transcription reactions using the mMMESSAGE mMACHINE SP6 kit (Ambion; AM1340) according to the manufacturer's instructions. Radiolabeled proteins were produced using rabbit reticulocyte lysate system (Promega; L4960) in the presence of [<sup>35</sup>S]-Methionine/Cysteine (Perkin Elmer). Translated protein was incubated at 37°C with isolated mitochondria resuspended in import buffer (250 mM sucrose, 5 mM magnesium acetate, 80 mM potassium acetate, 10 mM sodium succinate, 1 mM DTT, 5 mM ATP, 20 mM HEPES-KOH pH 7.4) in the presence or absence of 10  $\mu$ M FCCP to dissipate the membrane potential. Upon import, samples were treated with Proteinase K (50  $\mu$ g/mL for 10 minutes on ice) and PMSF (1 mM for 5 minutes on ice) prior to re-isolation for SDS-PAGE. Following import, mitochondria were prepared for and analyzed by SDS-PAGE and phosphorimaging.

### Proteomics analysis

Stable isotope labeling of amino acids in cell culture (SILAC) was performed as described (Dibley et al., 2020; Stroud et al., 2016). BioID proteomics was performed as previously described (Osellame et al., 2016). Affinity enrichment proteomic analysis was performed as previously described (Thompson et al., 2018).

### Mass spectrometry of SILAC treated cells

Mitochondria were isolated as above from COA1<sup>KO</sup> cells cultured in SILAC DMEM and prepared as described previously (Stroud et al., 2016). Mitochondrial protein yield was assayed by BCA. For each triplicate set, two replicates containing 50  $\mu$ g of protein from heavy labeled mitochondria were mixed with the same amount of protein from light KO mitochondria. The third replicate consisted of a label switch. Mitochondrial samples were treated as follows: Samples were solubilized in 1% (w/v) SDC, 100 mM Tris-Cl pH 8.1, 40 mM chloroacetamide and 10 mM TCEP prior to vortexing and heating for 5 minutes at 99°C with 1500 rpm shaking. Samples were then sonicated for 15 minutes in a room temperature water bath prior to the addition of 1  $\mu$ g trypsin (Promega; V5113) and incubation overnight at 37°C. The supernatant was then transferred to 3x 14G 3M<sup>TM</sup>Empore<sup>TM</sup> SDB-RPS stage tips (Kulak et al.,

2014). Ethyl acetate (99%) and 1% TFA was added to the tip before centrifugation at 3000 *g* at room temperature as described (Kulak et al., 2014). Stage tips were washed first with 99% ethyl acetate and 1% TFA and then with ethyl acetate supplemented with 0.2% TFA. Samples were eluted in 80% acetonitrile (ACN) and 1% NH<sub>4</sub>OH, and acidified to a final concentration of 1% TFA prior to drying in a SpeedVac.

### Mass-spectrometry and data analysis

Peptides were reconstituted in 2% ACN, 0.1% TFA and transferred to autosampler vials for analysis by online nano-HPLC/electrospray ionization-MS/MS on either a Thermo-Fisher Scientific Orbitrap Q Exactive Plus, Orbitrap Fusion Lumos Tribrid or Orbitrap Elite Hybrid Ion-Trap instrument as follows:

NDUFAF1<sup>BirA\*</sup>, TMEM186<sup>Flag</sup> and COA1<sup>Flag</sup> AE-MS were acquired on an Orbitrap Elite Hybrid Ion-Trap instrument connected to an Ultimate 3000 HPLC (Thermo-Fisher Scientific). Peptides were loaded onto a trap column (PepMap C18 trap column 75 μm x 2 cm, 3 μm, particle size, 100 Å pore size; ThermoFisher Scientific) at 5 μL/min for 3 min before switching the pre-column in line with the analytical column (PepMap C18 analytical column 75 μm x 50 cm, 2 μm particle size, 100 Å pore size; ThermoFisher Scientific). Peptide separation was performed at 300 nL/min using a 90 min non-linear ACN gradient of buffer A [0.1% (v/v) formic acid, 2% (v/v) ACN, 5% DMSO] and buffer B [0.1% (v/v) formic acid in ACN, 5% DMSO]. Data was collected in Data Dependent Acquisition (DDA) mode using m/z 300 - 1650 as MS scan range, rCID for MS/MS of the 20 most intense ions. Other instrument parameters were: MS scan at 120,000 resolution, maximum injection time 150 ms, AGC target 1E6, CID at 30% energy for a maximum injection time of 150 ms with AGC target of 5,000.

For COA1<sup>KO</sup> mitochondria, data were acquired on an Orbitrap Fusion Lumos instrument connected to an Ultimate 3000 HPLC. Peptides were loaded onto a trap column (PepMap C18 trap column 75 μm x 2 cm, 3 μm, particle size, 100 Å pore size; ThermoFisher Scientific) at 5 μL/min for 3 min before switching the pre-column in line with the analytical column (PepMap C18 analytical column 75 μm x 50 cm, 2 μm particle size, 100 Å pore size; ThermoFisher Scientific). The separation of peptides for was performed at 300 nL/min using a 90 min non-linear ACN gradient of buffer A [0.1% (v/v) formic acid, 2% (v/v) ACN, 5% DMSO] and buffer B [0.1% (v/v) formic acid in ACN, 5% DMSO]. The mass spectrometer was operated in positive-ionization mode with spray voltage set at 1.9 kV and source temperature at 275°C. Lockmass of 401.92272 from DMSO was used. Data were collected using the Data Dependent Acquisition using m/z 350-1550 at 120000 resolution with AGC target of 5e5. The “top speed” acquisition method (3 s cycle time) on the most intense precursor was used whereby peptide ions with charge states ≥ 2-5 were isolated with isolation window of 1.6 m/z and fragmented with high energy collision (HCD) mode with stepped collision energy of 30 ± 5%. Fragment ion spectra were acquired in Orbitrap at 15000 resolution. Dynamic exclusion was activated for 30 s.

Raw files were analyzed using the MaxQuant platform (Tyanova et al., 2016a) version 1.6.5.0 searching against the UniProt human database containing reviewed, canonical entries (January 2019) and a database containing common contaminants. For label-free (LFQ) AE-MS experiments, default search parameters were used with “Label free quantitation” set to “LFQ” and “Match between runs” enabled. Using the Perseus platform (Tyanova et al., 2016b) version 1.6.7.0, proteins group LFQ intensities were Log<sub>2</sub> transformed. Values listed as being ‘Only identified by site’, ‘Reverse’ or ‘Contaminants’ were removed from the dataset. Mitochondrial annotations were imported by matching with the Mitocarta2 dataset (Calvo et al., 2016) by gene name and/or ENSG identifier and the Integrated Mitochondria Protein Index (IMPI) database by gene name (Smith and Robinson, 2019). Experimental groups were assigned to each set of triplicates and the number of valid values for row group calculated. For each experiment (containing a control and an enrichment group) rows having less than 3 valid values in the enrichment group were removed and the missing values in the relevant control group imputed to values consistent with the limit of detection. A modified two-sided Student’s t test based on permutation-based FDR statistics (Tyanova et al., 2016b) was performed between the two groups. The negative logarithmic *p*-values were plotted against the differences between the Log<sub>2</sub> means for the two groups. The significance threshold used for these experiments is noted in the relevant figure legend and supplementary tables. For SILAC experiments, default search parameters were used with multiplicity set to 2 (Lys8, Arg10) and “Match between runs” enabled. Using the Perseus platform (Tyanova et al., 2016b) version 1.6.7.0, proteins group normalized H/L ratios were Log<sub>2</sub> transformed. Label switched samples (L/H) were inverted to KO/HEK293T orientation prior to this step. Values listed as being ‘Only identified by site’, ‘Reverse’ or ‘Contaminants’ were removed from the dataset. Mitochondrial annotations were imported by matching with the Mitocarta2 and IMPI datasets as above. Experimental groups were assigned to each set of triplicates rows with < 2 valid values for each group removed. Non-mitochondrial proteins were removed, and a one sample Student’s two-sided t test was performed within each group. The negative logarithmic *p*-values were plotted against the differences between the mean ratios for each group. A significance threshold (*p* < 0.05) was used for all experiments. Log<sub>2</sub>-transformed median SILAC ratios were mapped on homologous subunits of the respiratory chain complexes. Applicable Protein Data Bank accession codes provided in text.

### QUANTIFICATION AND STATISTICAL ANALYSIS

Band intensities from western blots were measured using ImageLab 5.2.1 (BioRad) by measuring band intensity and subtracting a background measurement away from the region of interest. Band intensities were normalized to the intensity of an independent band and taken as a percentage of the control as indicated. Values were then analyzed in GraphPad Prism 7.01. Results are reported as the mean ± SEM from three independent experiments. Statistical details can be found in the associated figure legends.

SILAC analyses were performed in triplicate, with a label switch as we have done previously (Dibley et al., 2017; Stroud et al., 2015, 2016). The statistical approaches used to analyze the data was consistent with published quantitative SILAC analyses from our (Stroud et al., 2015, 2016) and other labs employing similar instrumentation and methods. Statistical analysis was performed using the Perseus platform (Tyanova et al., 2016b). For steady-state analysis the fold change threshold we used for significance was  $> 1.5$  and a  $p < 0.05$  following a single sample two-sided Student's t test. AE-MS analyses were performed in triplicate using label free quantitation and compared to untagged control cells as we (Lim et al., 2018) and others have done previously using similar instrumentation and methods. Imputation was performed only on missing values in control samples and random values were drawn from a narrow distribution equivalent to the limit of detection of the instrument. Significantly-enriched proteins were determined through a modified two-sample two-sided Student's t test based on permutation-based FDR statistics (Tyanova et al., 2016b) between the two groups, with an FDR of 1% and the  $s_0$  value determined iteratively to exclude any enriched proteins specific to the control group.

### DATA AND CODE AVAILABILITY

The mass spectrometry proteomics data have been deposited to the ProteomeXchange Consortium via the PRIDE (Perez-Riverol et al., 2019) partner repository with the dataset identifier PRIDE: PXD018075.



Minerva Access is the Institutional Repository of The University of Melbourne

**Author/s:**

Formosa, LE; Muellner-Wong, L; Reljic, B; Sharpe, AJ; Jackson, TD; Beilharz, TH;  
Stojanovski, D; Lazarou, M; Stroud, DA; Ryan, MT

**Title:**

Dissecting the Roles of Mitochondrial Complex I Intermediate Assembly Complex Factors in the Biogenesis of Complex I

**Date:**

2020-04-21

**Citation:**

Formosa, L. E., Muellner-Wong, L., Reljic, B., Sharpe, A. J., Jackson, T. D., Beilharz, T. H., Stojanovski, D., Lazarou, M., Stroud, D. A. & Ryan, M. T. (2020). Dissecting the Roles of Mitochondrial Complex I Intermediate Assembly Complex Factors in the Biogenesis of Complex I. CELL REPORTS, 31 (3), <https://doi.org/10.1016/j.celrep.2020.107541>.

**Persistent Link:**

<http://hdl.handle.net/11343/273764>

**File Description:**

Published version

**License:**

CC BY-NC-ND